RESEARCH ARTICLE SUMMARY

GENE REGULATION

Lineage-specific enhancers activate self-renewal genes in macrophages and embryonic stem cells

Erinn L. Soucie,*† Ziming Weng,† Laufey Geirsdóttir,† Kaaweh Molawi,† Julien Maurizio, Romain Fenouil, Noushine Mossadegh-Keller, Gregory Gimenez, Laurent VanHille, Meryam Beniazza, Jeremy Favret, Carole Berruyer, Pierre Perrin, Nir Hacohen, J.-C. Andrau, Pierre Ferrier, Patrice Dubreuil, Arend Sidow,* Michael H. Sieweke*

INTRODUCTION: In many organs of the body, differentiated cells are frequently lost and need to be replaced as part of normal homeostatic tissue maintenance or in response to injury. In most cases, this regeneration is assured by differentiation from tissue-specific stem cells. Together with a few other cell types, tissue macrophages represent a rare exception to this pathway, as they can be maintained independently of blood stem cells by local proliferation. Under certain conditions, mature macrophages can also be expanded and maintained long term in culture without transformation or loss of differentiation status. The gene regulatory mechanisms that allow such differentiated cells to self-renew while maintaining cell type–specific identity have so far remained unknown. Self-renewing macrophages provide a rare opportunity to study this question.

RATIONALE: Molecularly, cell identity can be defined by the genomic positions of gene regulatory enhancer elements. The cell type–specific signatures and activity status of such elements have been characterized by the analysis of specific histone modifications and the binding of regulatory proteins. To identify the regulatory mechanisms that enable macrophage self-renewal capacity to be integrated into the overall program of epigenetic macrophage identity, we have compared the enhancer repertoires of quiescent and self-renewing macrophages. Based on our previous observations that deletion of MafB and c-Maf transcription factors results in an extended self-renewal capacity of macrophages, we further investigated how the absence of Maf transcription factors affects the enhancers of specific self-renewal genes and how these mechanisms activate macrophage self-renewal under homeostatic and challenge conditions in vivo.

RESULTS: Compared to quiescent macrophages, self-renewing macrophages showed no appreciable difference with respect to genome-wide enhancer positions but displayed an increase in the activation status of many enhancers that were also bound by the lineage-specifying transcription factor PU.1 in both cell types. This finding suggests that these poised macrophage-specific enhancers became active in self-renewing macrophages. We found activated enhancers to be associated with a network of genes, centered on *Myc* and *Klf2*, that were up-regulated and functionally important for self-renewal in these cells. The same genes were also required for embryonic stem (ES) cell self-renewal but were associated with a distinct, ES cell–specific set of enhancers. We observed that activated self-renewal–associated macrophage enhancers were directly repressed by MafB binding. The loss of MafB and c-Maf expression relieved this repression and led to activation of the self-renewal gene network in MafB and cMaf knockout macrophages, as well as in alveolar macrophages that express constitutively low levels of these transcription factors. In vivo single-cell analysis further revealed that, both in the steady state and in response to immune stimulation, proliferating resident macrophages could access this network by transient down-regulation of Maf transcription factors.

ON OUR WEB SITE

Read the full article at http://dx.doi.org/10.1126/science.aad5510

CONCLUSION: Our results demonstrate that self-renewal in macrophages involves down-regulation of MafB and cMaf, as well as concomitant activation of a self-renewal gene network shared with ES cells but controlled from cell type–specific enhancers. Macrophage enhancers associated with self-renewal genes are already present in quiescent cells and can become activated when direct repression by Maf transcription factors is relieved. Our findings provide a general molecular rationale for the compatibility of self-renewal and differentiated cell functions and may also be more generally relevant for the direct activation of self-renewal activity in other differentiated cell types with therapeutic potential. ■

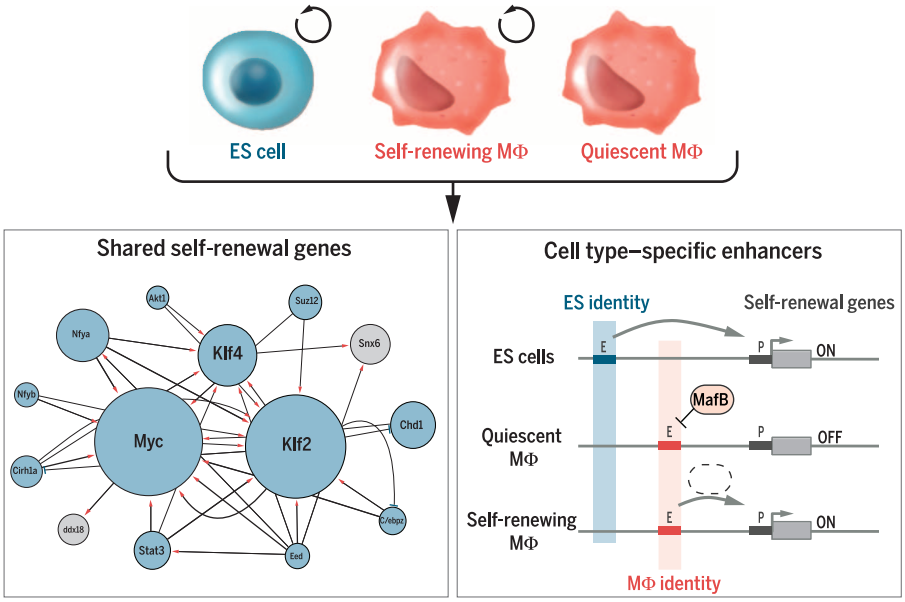

The self-renewal potential of both ES cells and differentiated macrophages is dependent on a shared network of self-renewal genes (**left**) that are controlled by distinct lineage-specific enhancers (**right**). In quiescent macrophages, the transcription factor MafB binds and represses these enhancers. The loss of MafB expression results in enhancer activation and enables macrophage self-renewal. At bottom left, red arrows indicate activation; blue bars represent inhibition. Circle size is a function of the number of times the target is affected by other regulators. MΦ, macrophage; E, enhancer; P, promoter.

The list of author affiliations is available in the full article online.
*Corresponding author. E-mail: sieweke@ciml.univ-mrs.fr (M.H.S.); erinn.soucie@inserm.fr (E.L.S.); arend@stanford.edu (A.S.)
†These authors contributed equally to this work.
Cite this article as E. L. Soucie *et al.*, *Science* **351**, aad5510 (2016). DOI: 10.1126/science.aad5510

RESEARCH ARTICLE

GENE REGULATION

Lineage-specific enhancers activate self-renewal genes in macrophages and embryonic stem cells

Erinn L. Soucie,[1,2,3,4]*† Ziming Weng,[5]† Laufey Geirsdóttir,[1,2,3]† Kaaweh Molawi,[1,2,3,6]† Julien Maurizio,[1,2,3] Romain Fenouil,[1,2,3] Noushine Mossadegh-Keller,[1,2,3] Gregory Gimenez,[1,2,3] Laurent VanHille,[1,2,3] Meryam Beniazza,[1,2,3] Jeremy Favret,[1,2,3] Carole Berruyer,[1,2,3] Pierre Perrin,[1,2,3] Nir Hacohen,[7] J.-C. Andrau,[1,2,3,8] Pierre Ferrier,[1,2,3] Patrice Dubreuil,[4] Arend Sidow,[5,9]* Michael H. Sieweke[1,2,3,6]*

Differentiated macrophages can self-renew in tissues and expand long term in culture, but the gene regulatory mechanisms that accomplish self-renewal in the differentiated state have remained unknown. Here we show that in mice, the transcription factors MafB and c-Maf repress a macrophage-specific enhancer repertoire associated with a gene network that controls self-renewal. Single-cell analysis revealed that, in vivo, proliferating resident macrophages can access this network by transient down-regulation of Maf transcription factors. The network also controls embryonic stem cell self-renewal but is associated with distinct embryonic stem cell–specific enhancers. This indicates that distinct lineage-specific enhancer platforms regulate a shared network of genes that control self-renewal potential in both stem and mature cells.

In many tissues of the body, differentiated cells are frequently replaced as part of homeostatic maintenance or in response to injury. Whereas in most cases this depends on tissue-specific stem cells, tissue macrophages can be maintained by local proliferation independently of hematopoietic stem cells (*1*–*4*), possibly by self-renewal mechanisms activated in mature macrophages (*5*). Unlike the few examples of differentiated normal cells that can transiently reenter the cell cycle, such as hepatocytes, macrophages can also be expanded and maintained in long-term culture without transformation or loss of differentiation. This has been observed in macrophages with deletions of two core macrophage transcription factors (*6*)—MafB and c-Maf [Maf double-knockout (Maf-DKO) macrophages] (*7*)—or in cultures derived from fetal progenitors (*8*).

Understanding how regulatory programs are rewired to allow differentiated cells to self-renew is of considerable interest, and self-renewing macrophages present a rare opportunity to study this process. Genome-wide distribution of enhancer-associated histone modifications provides a reliable signature of cell identity (*9*–*14*) that has revealed macrophage-specific enhancer repertoires (*11*, *12*) and tissue- or activation-state–dependent modifications (*15*–*17*). To identify the regulatory mechanism that enables macrophage self-renewal capacity to be integrated into the overall program of epigenetic macrophage identity, we therefore compared the enhancer repertoires of quiescent and self-renewing macrophages.

Absence of lineage-independent self-renewal enhancers

To determine whether self-renewal in macrophages involves acquisition of dedicated, self-renewal–specific enhancers, we first compared the molecular enhancer signature defined by monomethylated histone H3 at lysine 4 (H3K4m1) (*9*, *13*, *14*) of self-renewing Maf-DKO and quiescent wild-type (WT) bone marrow macrophages (BMMs) to several other cell types with limited proliferation or extended self-renewal capacity (fig. S1). Surprisingly, our analysis revealed no common, lineage-independent repertoire of shared enhancer positions for the control of proliferation or self-renewal genes (fig. S1, A and B). We also compared genome-wide binding of the transcription factor PU.1, a key regulator of both macrophage and B cell lineage identity that defines distinct enhancer positions in the genome of these two cell types (*10*–*12*). This revealed fewer differences in the position of H3K4m1$^+$/PU.1$^+$ enhancer peaks between Maf-DKO and WT BMMs than between WT BMMs and peritoneal macrophages (PMs), as well as an equal distance of all macrophage populations to pro-B cells (fig. S1C). This indicates that Maf-DKO macrophages can activate self-renewal but retain a macrophage-specific enhancer signature similar to that of WT BMMs. Thus, macrophage self-renewal does not appear to involve the acquisition of dedicated, lineage-independent self-renewal enhancers or the loss of mature macrophage epigenetic identity.

Activation of a lineage-specific subset of enhancers in self-renewing macrophages

Because self-renewing Maf-DKO macrophages showed no appreciable difference compared to quiescent macrophages with respect to genome-wide enhancer positions, we performed chromatin immunoprecipitation sequencing (ChIP-seq) analyses for activated enhancer marks; histone acetyl transferase p300; and the histone modification mediated by this enzyme, acetylation of H3K27 (H3K27ac) (*13*, *17*–*19*), to determine whether the activation status of these enhancers differed. We found that a large number of enhancers were activated specifically in Maf-DKO macrophages only (Maf-DKO-only) (Fig. 1A, red highlight), whereas a small number of enhancers were activated specifically in WT BMMs. Specifically, we calculated 7323 enhancer regions to be enriched for p300 binding and 7489 enriched for H3K27ac in Maf-DKO macrophages compared to WT BMMs, whereas only 305 regions were enriched for p300 and 1923 for H3K27ac in WT BMMs compared with Maf-DKO macrophages (Fig. 1B and fig. S2). Further characterization of Maf-DKO-only regions revealed a typical H3K4m1$^+$/H3K4m3^{low} enhancer signature at these loci (Fig. 1, A and C), and motif search analysis of the p300- and H3K27ac-enriched Maf-DKO-only enhancer regions revealed the highest score for PU.1 binding motifs (log P = 6444) (fig. S3A). Aggregate analysis of all PU.1-bound sites in Maf-DKO and WT macrophages confirmed that the large majority of DKO-only enhancers was bound by PU.1 (Fig. 1, B and C, and fig. S3B) and that more than 60% of these positions were also bound by PU.1 in WT macrophages (Fig. 1, B and C, and fig. S3B). This PU.1 binding pattern is reminiscent of "poised" and "latent" enhancers previously described in nonstimulated and stimulated macrophages, respectively (*17*). Taken together, macrophages appear to possess a specific subset of largely poised macrophage-specific enhancers that is selectively activated in self-renewing Maf-DKO macrophages.

Self-renewing macrophages activate a gene set also required for embryonic stem cell self-renewal

Under steady-state conditions, self-renewing Maf-DKO and WT BM macrophages have highly similar global gene expression profiles (*7*). However, it is possible that the global analysis hides relevant specific mechanisms, so we specifically selected the genes associated with Maf-DKO-only–activated enhancers for further study, using the Genomic Regions Enrichment of Annotations Tool (GREAT)

[1]Centre d'Immunologie de Marseille-Luminy, Université Aix-Marseille, UM2, Campus de Luminy, Case 906, 13288 Marseille Cedex 09, France. [2]INSERM, U1104, Marseille, France. [3]CNRS, UMR 7280, Marseille, France. [4]Centre de Recherche en Cancerologie de Marseille, INSERM (U1068), CNRS (U7258), Université Aix-Marseille (UM105), Marseille, France. [5]Department of Pathology, Stanford University, Stanford, CA 94305-5324, USA. [6]Max-Delbrück-Centrum für Molekulare Medizin in der Helmholtz-Gemeinschaft, 10 Robert-Rössle-Strasse, 13125 Berlin, Germany. [7]Broad Institute of Harvard University and MIT, Cambridge, MA 02142, USA. [8]Institut de Génétique Moléculaire de Montpellier, CNRS UMR 5535, 1919 Route de Mende, 34293 Montpellier, France. [9]Department of Genetics, Stanford University, Stanford, CA 94305, USA.
***Corresponding author. E-mail: sieweke@ciml.univ-mrs.fr (M.H.S.); erinn.soucie@inserm.fr (E.L.S.); arend@stanford.edu (A.S.)** †These authors contributed equally to this work.

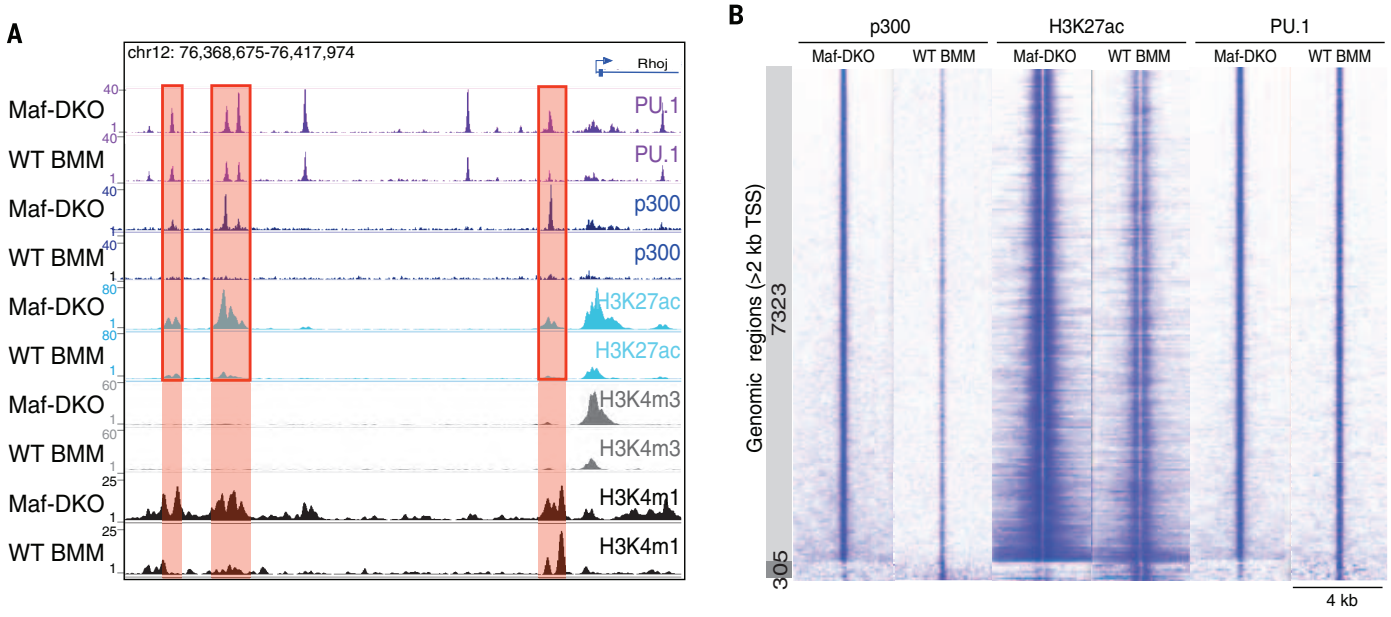

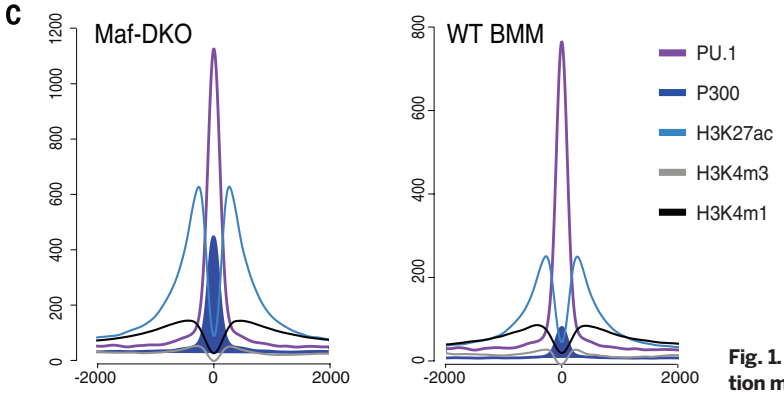

Fig. 1. A subset of lineage-specific enhancers are enriched for activation marks in self-renewing Maf-DKO macrophages. (**A**) Representative predicted enhancer regions (red shading), with greater enrichment for enhancer activation marks p300 and H3K27ac in Maf-DKO macrophages versus WT BMMs (red boxes). (**B**) Direct alignment of p300, H3K27ac, and PU.1 ChIP-seq signals for enhancer regions differentially enriched for p300 marks in Maf-DKO macrophages (7323, light gray) and WT BMMs (305, dark gray), centered and ranked on the p300 signal. (**C**) Aggregation plots showing average ChIP-seq signals for PU.1, H3K27ac, p300, H3K4m1, and H3K4m3 marks in Maf-DKO and WT BMMs for p300 regions specifically enriched in Maf-DKO macrophages [depicted in light gray in (B)]. For each protein target, results of ChIP-seq analysis were reproducible in at least two biological replicates. (**D**) Microarray gene expression ratios of Maf-DKO versus WT BMMs 2 hours after M-CSF stimulation, for total genes (white) or genes associated with Maf-DKO-only enhancers (blue). The box extends from the first to the third quartile, with the whiskers denoting 1.5 times the interquartile range. Data were derived from three biological replicates.

(*20*). We observed a specific increase in the expression of these genes after stimulation with macrophage colony-stimulating factor (M-CSF), a cytokine required to maintain self-renewal (*7*) (Fig. 1D). This indicates that Maf-DKO macrophage–activated enhancers comprise elements conferring functional responsiveness to M-CSF stimulation, potentially including those relevant to self-renewal. Gene Ontology (GO) analysis on Maf-DKO-only–associated genes revealed immune and myeloid cell functions (fig. S3C) but no groups associated with self-renewal activity. Because GO lacks self-renewal–specific categories, we performed Gene Set Enrichment Analysis (GSEA) on the Maf-DKO-only–associated genes, using both adult and embryonic stem (ES) cell–specific data modules enriched for self-renewal genes (*21*). This analysis revealed a significant enrichment of the ES cell but not the adult stem cell set in Maf-DKO over WT BM macrophage expression (Fig. 2A). On the basis of these results, we focused on functionally validated genes identified in screens for self-renewal activity in ES cells (*22*–*29*). Although the identified list of 53 genes from these screens (Fig. 2B) is not likely to be exhaustive, it constitutes the largest functionally validated gene set available that should include core elements of self-renewal activity. The genes on this list fall into two categories: those affecting self-renewal only (25 genes) and those affecting both self-renewal and pluripotency, as inferred by their influence on expression of *Oct4* or *Nanog* genes (28 genes) (Fig. 2B). Of the 25 genes in the self-renewal category, 15 (60%) were also associated with Maf-DKO-only enhancers in macrophages; of the 28 pluripotency genes, only one (4%), Chd1, also had an activated enhancer signature in Maf-DKO macrophages (Fig. 2B, red type). Similar results were obtained when the selection of self-renewal genes was based on transcription factor cross-regulatory circuits and interactome data in ES cells (*30*): None of the factors in an ES cell transcriptional cross-regulatory circuit belonging to the nanog interactome (0 of 10) and 6 of 11 (55%) genes in the network not interacting with nanog were activated in Maf-DKO macrophages (fig. S4). Our analysis revealed increased expression in Maf-DKO macrophages compared with WT BM macrophages for all 16 self-renewal genes associated with Maf-DKO-only–activated enhancers. This effect was enhanced in response to M-CSF (Fig. 2C).

Self-renewal genes are organized in a network and functionally important

To further investigate whether self-renewal genes in Maf-DKO macrophages were functionally integrated in a network of cross-regulated genes,

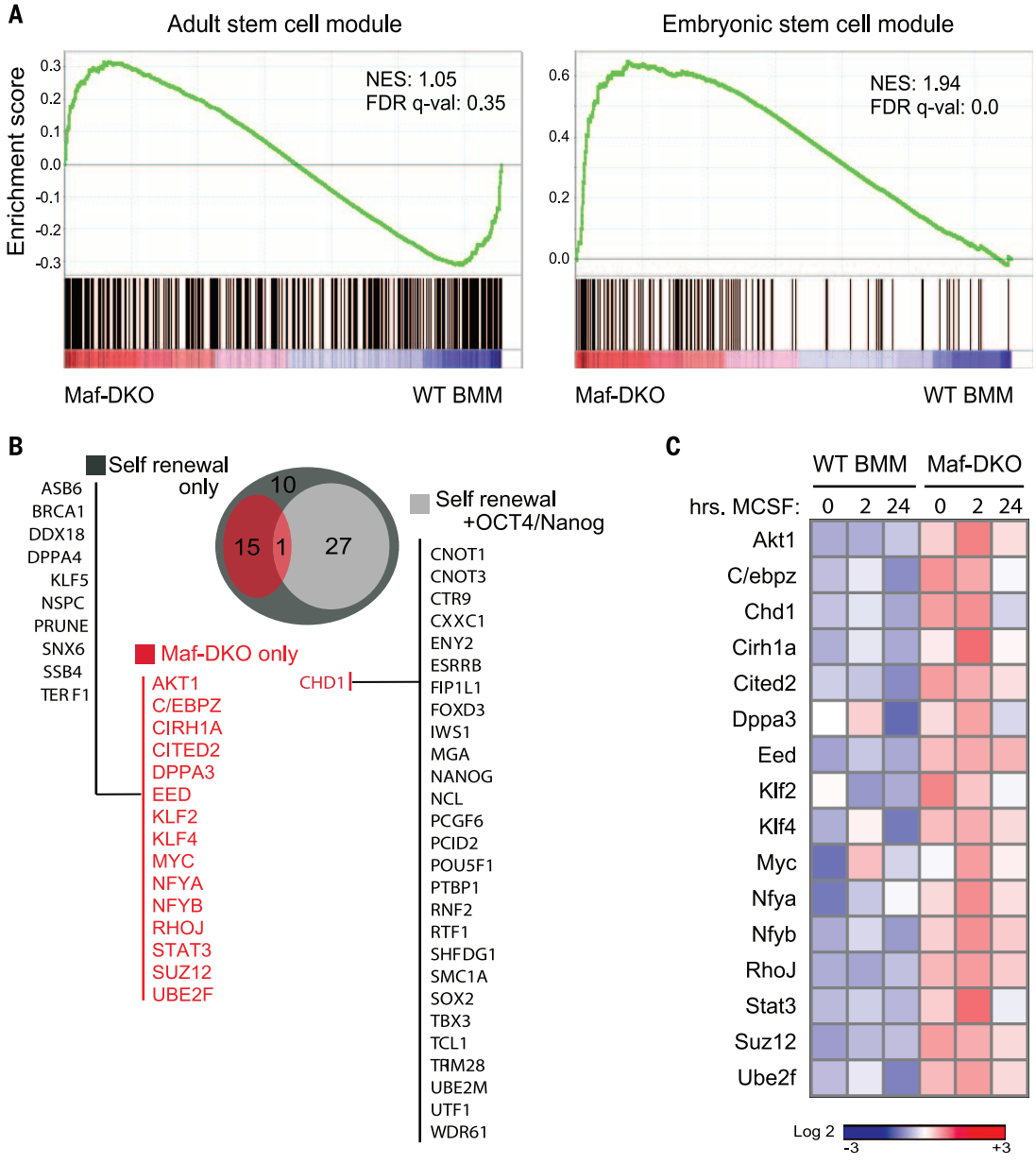

Fig. 2. Self-renewing Maf-DKO macrophages activate genes required for ES cell self-renewal. (**A**) Gene set enrichment analysis (GSEA) using gene sets defined by Wong *et al*. (*21*) for adult tissue stem cells and core ES cell modules (Broad Institute MSigDB M1999 and M7079), comparing the expression of genes associated with Maf-DKO-only–associated enhancers in Maf-DKO versus WT BMMs. NES, normalized enrichment score; FDR, false-discovery rate. (**B**) Diagram of overlapping groups of genes associated with Maf-DKO-only–activated enhancers (red) and functionally validated self-renewal (dark gray) or both self-renewal and pluripotency (self-renewal + Oct4/nanog; light gray) activity in ES cells, demonstrated by gene inactivation screens (*22*–*29*). (**C**) Gene expression by quantitative real-time PCR of self-renewal genes in Maf-DKO macrophages and WT BMMs stimulated with M-CSF for the indicated times. The heat map shows the average signal of technical replicates. Data are representative of four independent experiments.

we measured the effect of silencing individual self-renewal genes on the expression of other self-renewal genes. For 12 of the 16 identified self-renewal genes, validated short hairpin RNA (shRNA) vectors were available (*31*). In each knockdown, we measured the expression of 13 self-renewal genes associated with Maf-DKO-only macrophage enhancers and four additional self-renewal genes that might be regulated indirectly as part of a larger network. We also included probes against myeloid and housekeeping control genes (Fig. 3A). Knockdown of self-renewal genes only minimally influenced myeloid gene expression (Fig. 3A). By contrast, in all cases self-renewal–specific shRNAs substantially reduced not only the expression of their specific target but also that of other self-renewal genes. These analyses revealed a network of self-renewal gene regulation with Myc and Klf2 as the two main nodes and Klf4 as a minor node (Fig. 3B).

To determine whether the identified network of self-renewal genes was functionally important for self-renewal activity in Maf-DKO macrophages, we analyzed the effect of silencing individual self-renewal genes on colony-forming ability. We observed a significant reduction in Maf-DKO colony-forming units (CFUs) upon expression of at least one self-renewal gene–specific shRNA per gene compared with control (shLacz) for all vectors except Eed, which produced inconclusive results between different shRNA constructs and repeat experiments (Fig. 3C and fig. S5). We did not observe any significant effect of self-renewal gene silencing on apoptosis, as indicated by Annexin V and intracellular propidium iodine labeling (fig. S5B). The strongest effects on self-renewal were observed in the knockdowns of genes that occupy a central position in the network (Klf2/Myc). We observed weaker effects for several genes with peripheral positions (for example, Suz12), indicating that the knockdown of a single peripheral gene in the network might not be sufficient to compromise the activity of the entire self-renewal network.

Shared self-renewing genes have distinct enhancers in ES cells and macrophages

Our results indicated that self-renewal of Maf-DKO macrophages depends on an integrated network of cross-regulated self-renewal genes that are also employed for self-renewal in ES cells. To investigate how these very different cell types could access a similar gene network, we compared the gene regulatory mechanics

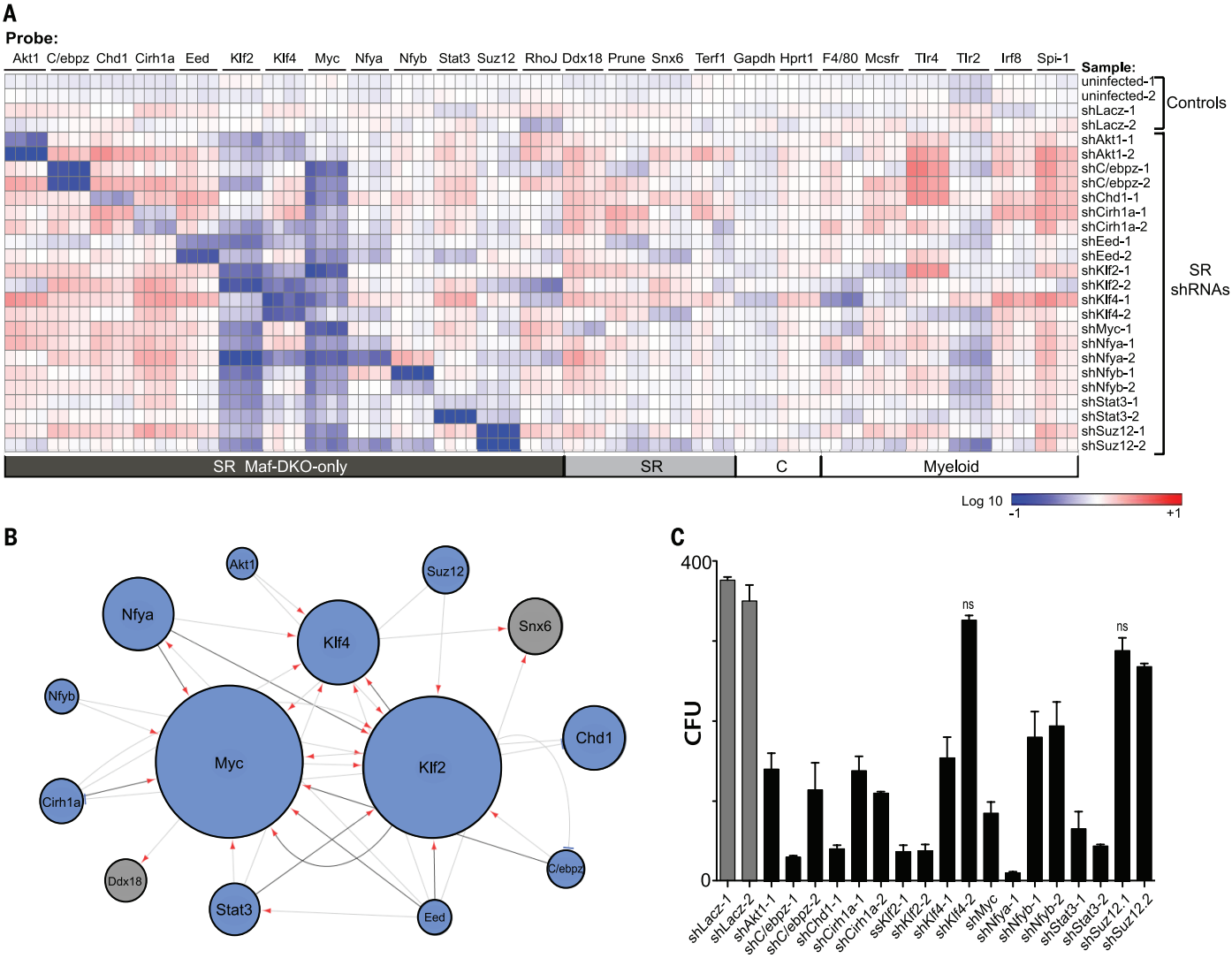

Fig. 3. Self-renewal genes are organized in a network and functionally important for Maf-DKO macrophage proliferation. (**A**) Gene expression analysis of Maf-DKO macrophages uninfected or infected with shLacZ control or shRNAs targeting self-renewal genes (rows) for self-renewal genes associated with Maf-DKO macrophage–activated enhancers, unassociated self-renewal genes (SR), housekeeping (C), and macrophage-specific (myeloid) genes (columns) using quadruplicate nanofluidic real-time PCR on Fluidigm array. For each gene, the heat map presents normalized values as percent change over average expression in noninfected and control lacZ shRNA–infected cell samples. Data are representative of three independent experiments. (**B**) Network model using an FDR approach, showing statistically significant repression of an output target gene resulting from shRNA knockdown of a regulator gene. Darker lines denote regulation in all replicates, red arrows indicate repression, and blue bars represent activation by shRNA. Circle size is a function of the number of times the target is affected by knockdown of other regulators. (**C**) Number of CFUs obtained from equal numbers of Maf-DKO macrophages infected with shRNAs against control (shLacZ) or self-renewal gene targets after 12 days of culture in MethoCult medium containing M-CSF. The mean number of CFUs for self-renewal gene shRNA–infected populations is significantly different from the mean number of CFUs for controls (one-way analysis of variance, $P < 0.05$) unless indicated (ns, not significant). Error bars represent SD of triplicate technical replicates, and data are representative of three independent experiments.

underlying activation of self-renewal genes in Maf-DKO macrophages and ES cells. As expected from the previous data and the differentiated phenotype of macrophages, genes affecting both self-renewal and pluripotency in ES cells, such as Oct4/POU5F1, showed activated enhancers in ES cells but not in macrophages (fig. S6A). By contrast, active enhancer elements were found to be associated with the genes of the identified self-renewal network both in ES cells and Maf-DKO macrophages (Fig. 4). However, the two cell types use entirely distinct sets of enhancers to activate these genes. The examples for the central factors Myc, Klf2, and Klf4 (Fig. 4A) and further network elements (fig. S6B) illustrate that ES cell–specific H3K27ac$^+$/p300$^+$ enhancers (blue in Fig. 4A and fig. S6B) and macrophage-specific H3K27ac$^+$/ p300$^+$ enhancers (red in Fig. 4A and fig. S6B) exist for each gene. To address these observations quantitatively, we identified the regulatory regions marked by H3K27ac in the three cell types (ES cells, Maf-DKO macrophages, and WT BMMs) for each of the known 16 self-renewal genes (Fig. 2B). To do this, we used a multisample-calling strategy to capture all shared regions and strong cell type–specific regions (Fig. 4B). There were 152 such regions, ranging from one region per gene (four genes) to 34 (*Cited2*), with an average of 9.5 and a median of 5. Genome browser inspection revealed almost completely nonoverlapping sets of active enhancer regions in macrophages and ES cells (Fig. 4A and fig. S6B). Consistent with these observations, we could identify two distinct enhancer clusters by *k*-means clustering ($k = 2$ clusters), where the most important characteristic separating the clusters is whether an enhancer is active in ES cells or in macrophages (Fig. 4B). The median normalized signal for enhancers in cluster one is 62 times higher in ES

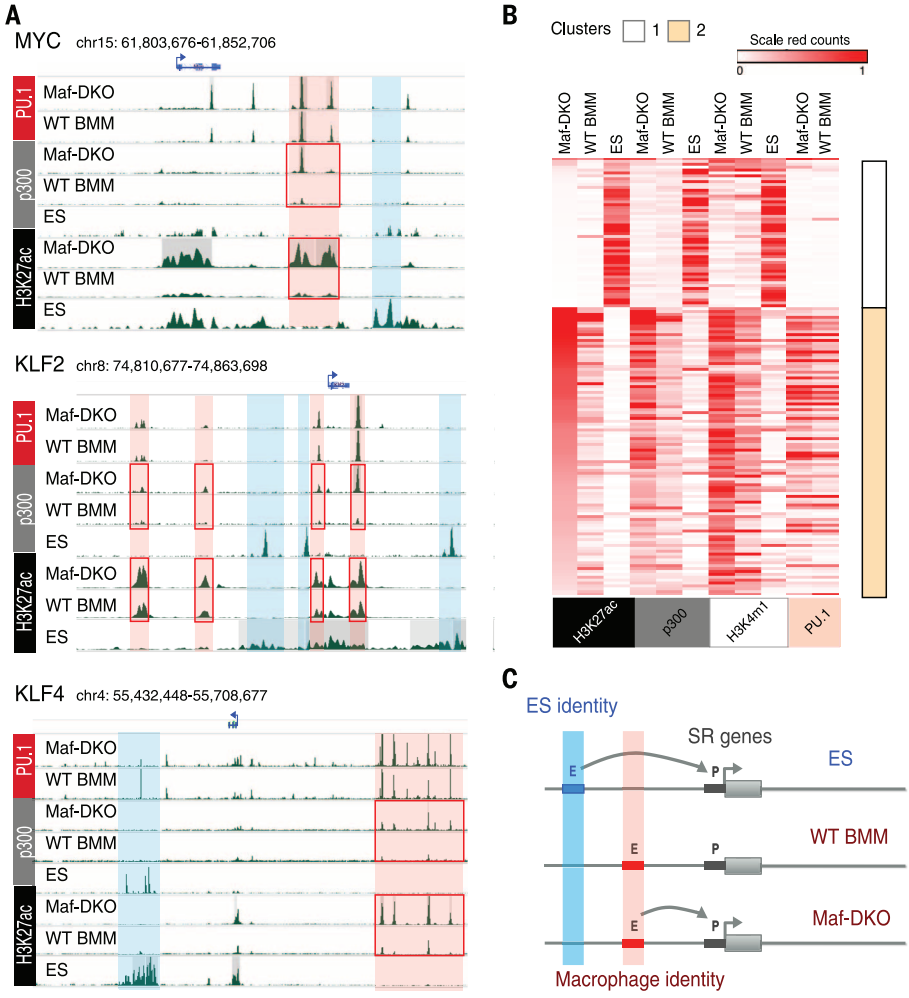

Fig. 4. Self-renewal genes are associated with distinct enhancers in ES cells and macrophages. (**A**) Genomic regions surrounding the *Myc*, *Klf2*, and *Klf4* genes, showing distinct ES cell– (blue) and macrophage- (red) specific predicted enhancer regions with differential H3K27ac and p300 enrichment in Maf-DKO over WT BMMs (red boxes). (**B**) Heat maps and *k*-means clustering ($k = 2$) of ChIP-seq signals of all H3K27ac^{+} regions associated with self-renewal genes in ES cells, Maf-DKO macrophages, and WT BMMs, including both differentially regulated Maf-DKO-only areas and nondifferentially regulated regions. Corresponding regions are shown for p300, H3K4m1, and PU.1 (ES, Maf-DKO macrophages, and WT BMMs). Read counts were individually scaled to the 95th percentile of each antibody signal. (**C**) Model to describe tissue-specific macrophage and ES cell–enhancer platforms associated with individual self-renewal genes. Color code is same as in (A). E, enhancer; P, promoter.

cells than in Maf-DKO macrophages; conversely, in cluster two the median normalized signal is 16 times higher in Maf-DKO macrophages than in ES cells. These patterns are mirrored at high statistical significance (*P* values ranging from 1.4×10^{-9} to 9.6×10^{-16}) in the ChIP-seq data from p300 and H3K4me1 (Mann-Whitney test), which had not been used in the clustering (Fig. 4B). Furthermore, enhancers associated with macrophage-specific self-renewal genes were 85 and 73% PU.1-positive in Maf-DKO and WT BM macrophages (Fig. 4B), indicating that macrophage self-renewal activates largely poised macrophage-specific enhancers. These results attest to the strong contrast among the clusters and their constituent regions and support the model that the same self-renewal genes can be accessed by distinct lineage-specific enhancer elements in two different cell types with self-renewal capacity (Fig. 4C).

MAFB directly represses self-renewal enhancers in macrophages

To better understand the mechanism leading to the activation of self-renewal enhancers in macrophages, we reexpressed MafB in Maf-DKO macrophages. MafB expression resulted in the reduction of both colony size and number in CFU assays (Fig. 5A), strongly inhibited expression of self-renewal genes (Fig. 5B), and reestablished low levels of p300 binding and H3K27ac modification, similar to WT BMMs at both Maf-DKO-only (fig. S7A) and self-renewal gene–associated enhancers (Fig. 5C). We further analyzed whether this rescue effect was due to a direct effect of MAFB on self-renewal gene–associated enhancers. Transcription factor binding sites enriched at Maf-DKO-only and, more specifically, self-renewal enhancers included Maf (MARE) and related AP-1 family binding sites (figs. S3A and S8). Furthermore, MAFB can also bind directly to PU.1 (*32*) and might thus target PU.1-positive enhancers by protein-protein interactions in the absence of consensus MARE. ChIP-seq analysis for MAFB in reconstituted Maf-DKO macrophages showed direct binding of MAFB (Fig. 5D) to 65% of PU.1-positive DKO-only enhancers and 73% of self-renewal gene–associated enhancers (Fig. 5E), as exemplified for the core factors of the network: Myc, Klf2, and Klf4 (Fig. 5F and fig. S7B). Similar binding profiles were observed for ChIP-seq analysis of endogenous MAFB in WT BMMs (fig. S9). Together, these results indicate that the activation of self-renewal is reversible and that the large majority of poised self-renewal–associated macrophage enhancers are directly repressed by MAFB binding.

Naturally low Maf levels in alveolar macrophages activate self-renewal enhancers

To further investigate whether our observations in Maf-DKO macrophages were directly relevant to the self-renewal capacity of genetically unmodified macrophages, we investigated alveolar macrophages (AMs). AMs are a population of adult resident macrophages that have the ability to autonomously self-renew (*4*) and that naturally express low levels of MafB and cMaf (*6*). Consistent with the constitutively low Maf levels compared with those of other macrophage populations (Fig. 6A and fig. S10), we could expand AMs in long-term liquid culture (Fig. 6B) and serially replate AMs, but not peritoneal macrophages (PMs), in colony-forming assays without losing replicative ability (Fig. 6C). Cultured AMs also expressed generally increased levels of self-renewal network genes (Fig. 6D). Furthermore, ChIP-seq analysis of epigenetic enhancer marks at the self-renewal gene–associated enhancer regions showed comparable binding of PU.1 between AMs, Maf-DKO macrophages, and WT BM macrophages but an enrichment of the activation mark p300 in AMs, as in Maf-DKO macrophages (Fig. 6, E and F). Statistical analysis confirmed a high correlation for PU.1 binding across all three populations and a high correlation for p300 binding between AMs and Maf-DKO macrophages but not BMMs (Fig. 6G). Thus, both experimental and natural reduction of MafB and c-Maf levels activates a set of poised macrophage-specific enhancers of the self-renewal gene network.

Low MafB levels activate self-renewal genes in resident macrophages in vivo

Many resident macrophage populations show a low level of local proliferation in vivo. Using immunofluorescence, we observed that the large majority of cycling, Ki67-positive macrophages in the peritoneum, liver, and spleen red pulp did not express MafB, whereas quiescent, Ki67-negative macrophages were nearly all MafB-positive (Fig. 7,

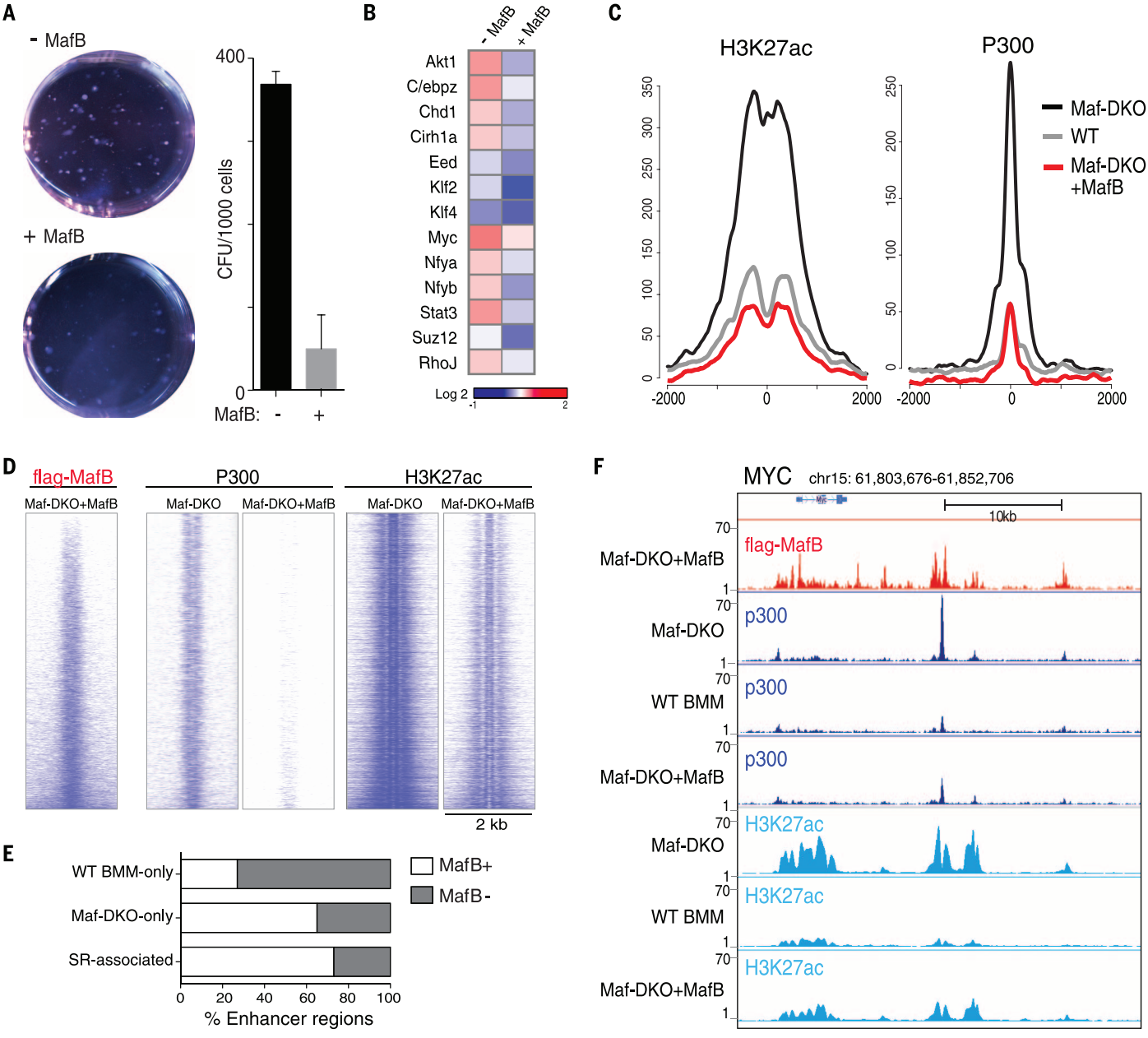

Fig. 5. MafB inhibits macrophage self-renewal by direct repression of self-renewal gene enhancers. (**A**) Colony assays for Maf-DKO macrophages expressing empty vector (−MafB) or a doxycycline-inducible Flag-tagged MafB allele (+MafB). Colonies were counted after 14 days of culture in MethoCult medium containing M-CSF and doxycycline. Culture dishes (0.63x) are shown at left, number of CFUs at right. Error bars represent SD of replicates, and data are representative of three independent experiments. $^{**}P$ = 0.004 by two-tailed, unpaired *t* test. (**B**) Expression of self-renewal genes in empty-vector Maf-DKO macrophages (−MafB) and Maf-DKO macrophages expressing a doxycycline-inducible, Flag-tagged MafB allele (+MafB), after 2 hours of stimulation with M-CSF, determined by nanofluidic real-time PCR on a Fluidigm array. Data are representative of three independent experiments. (**C**) Aggregation plots showing average ChIP-seq signals for P300 and H3K27ac in Maf-DKO macrophages expressing empty vector, WT BMMs, and Maf-DKO macrophages expressing a doxycycline-inducible, Flag-tagged MafB allele in the presence of doxycycline (Maf-DKO+MafB) for the self-renewal–associated enhancer regions (total = 88 regions). (**D**) Direct alignment of regions proximal to Maf-DKO-only enhancers for Flag-MAFB binding in Maf-DKO+MafB and corresponding regions in Maf-DKO and Maf-DKO +MafB macrophages for P300 and H3K27ac binding. (**E**) Histogram showing the percent of WT BMM-only–, Maf-DKO-only–, and self-renewal gene–associated enhancers bound by MAFB, as determined by ChIP-seq for Flag-MAFB in Maf-DKO+MafB cells. (**F**) Genomic regions surrounding the *Myc* gene with ChIP-seq tracks as labeled.

A and B; fig. S11; and table S1), indicating that macrophage proliferation in vivo also involved reduced MafB levels. Resident macrophages can further expand massively by transient local proliferation in response to specific stimuli (*5*, *33*)—for example, to M-CSF during infection of the peritoneum (*34*, *35*), which can be mimicked by direct intraperitoneal injection of the cytokine (*34*, *35*) (fig. S12). To address whether under such conditions macrophages could access the self-renewal gene network by transient repression of MafB and/or cMaf, we measured both self-renewal gene expression and MafB and cMaf expression before and at various time points after M-CSF stimulation by single-cell analysis of sorted resident peritoneal macrophages. One hour after stimulation, we observed a transient reduction of MafB (Fig. 7C) and, to a much lesser

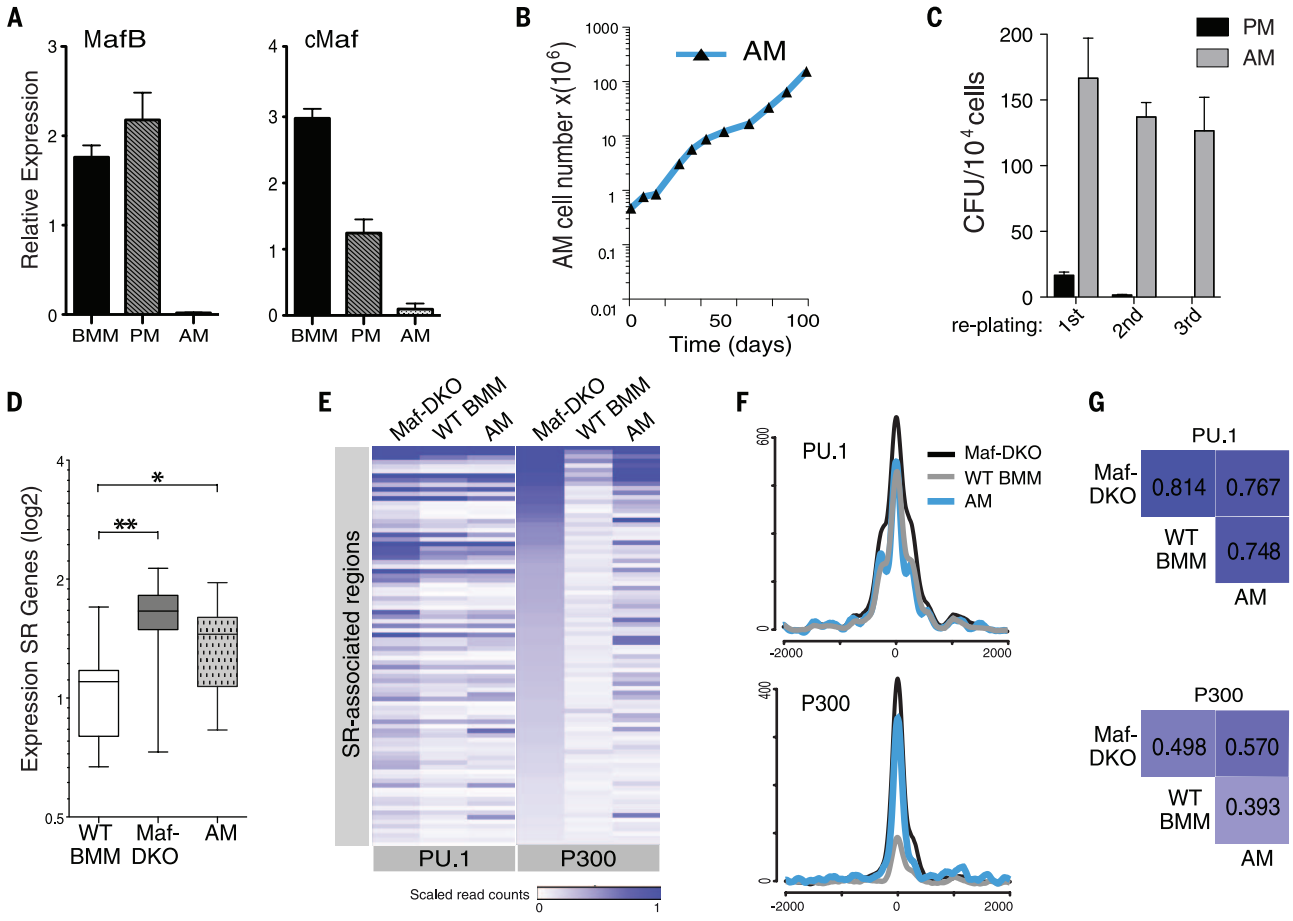

Fig. 6. The self-renewal gene network is activated in AMs expressing naturally low levels of MafB and cMaf. (**A**) Expression of MafB and cMaf relative to HPRT1, measured by RT-QPCR, in short-term cultures of BMMs, PMs, and AMs. Error bars represent SD of replicates, and data are representative of three independent experiments using biological replicates. (**B**) Growth curve showing number of AMs over time in liquid culture. Data are representative of two independent experiments. (**C**) Number of CFUs counted at day 21 per 10^4 AMs and PMs plated in MethoCult medium after the first plating, after replating 10^4 cells washed out from the first plating (2nd plating), or after the second plating (3rd plating). Error bars represent SD of replicates, and data are representative of three independent experiments. (**D**) Box plots showing average, interquartile, and 5th to 95th percentile relative expression levels of all self-renewal genes in Maf-DKO macrophages, WT BMMs, and AMs, as measured by nanofluidic real-time PCR on a Fluidigm array. *$P < 0.05$; **$P < 0.01$ (based on an unpaired t test). Data are based on the average signal from three biological replicates, each performed with technical duplicate. (**E**) Heat map of ChIP-seq signals for all regions associated with self-renewal genes (total = 88) in Maf-DKO macrophages, WT BMMs, and AMs. Corresponding regions are shown for PU.1 and P300, and read counts were individually scaled to the 95th percentile of each antibody signal. (**F**) Aggregation plots showing average ChIP-seq signals for PU.1 and P300 in Maf-DKO macrophages, WT BMMs, and AMs for the self-renewal–associated enhancer regions (total = 88 regions). (**G**) Pearson correlation matrix (PCA ranked $\log_2$ read number) for PU.1 and P300 binding to self-renewal gene–associated enhancers (total = 88 regions), based on ChIP-seq data for Maf-DKO macrophages, WT BMMs, and AMs. ChIP-seq analysis on AMs for PU.1 and p300 was performed twice.

extent, of c-Maf but not of control myeloid genes (fig. S13A). Reasoning that the behavior of resident peritoneal macrophages might be heterogeneous, we could identify three distinct groups of cells by principal component analysis (PCA) and *k*-means clustering (Fig. 7D). Whereas cells in cluster three were equally present before and after stimulation, cluster-two cells were strongly reduced and cluster-one cells strongly increased after M-CSF stimulation (Fig. 7E). Cells in cluster two expressed high levels of MafB and c-Maf but were negative for nearly all self-renewal genes. By contrast, cells in cluster one showed low MafB levels and up-regulation of the large majority of self-renewal genes (Fig. 7F). Cluster-three cells also showed high MafB levels (fig. S13B). Direct comparison of the expression of MafB and Myc in individual cells revealed a large number of cells with high MafB and low Myc levels in clusters two and three (fig. S13C). By contrast, a majority of cells in cluster one showed low or absent MafB levels and high levels of Myc (Fig. 7G). This analysis also demonstrated that a few cells with a MafB-low/Myc-high profile already existed in the steady state but their number strongly increased after M-CSF stimulation (Fig. 7G).

Overall, our results demonstrate that down-regulation of MafB and cMaf and concomitant activation of a self-renewal gene network is a hallmark of proliferating resident macrophages in culture and in vivo. Natural or experimentally induced constitutively low levels of MafB and c-Maf also enable long-term continuous self-renewal of adult macrophages in culture, as observed for AMs or Maf-DKO macrophages, respectively. Although inactivation of type I interferon signaling has also been associated with increased macrophage proliferation (*36*), we could not identify a direct link between Maf activity and this pathway. Furthermore, repression of interferon-β by MafB has been reported (*37*), which is the opposite of what would be expected if Maf transcription factors acted through interferons to limit macrophage proliferation.

We show that a network of genes that governs macrophage self-renewal overlaps substantially with that controlling self-renewal in ES cells. The regulatory mechanism by which activation of these genes is accomplished involves almost entirely separate sets of enhancers in the two cell types. The identified enhancer architecture associated with self-renewal genes in macrophages is already present in quiescent cells and can become activated when direct repression by Maf

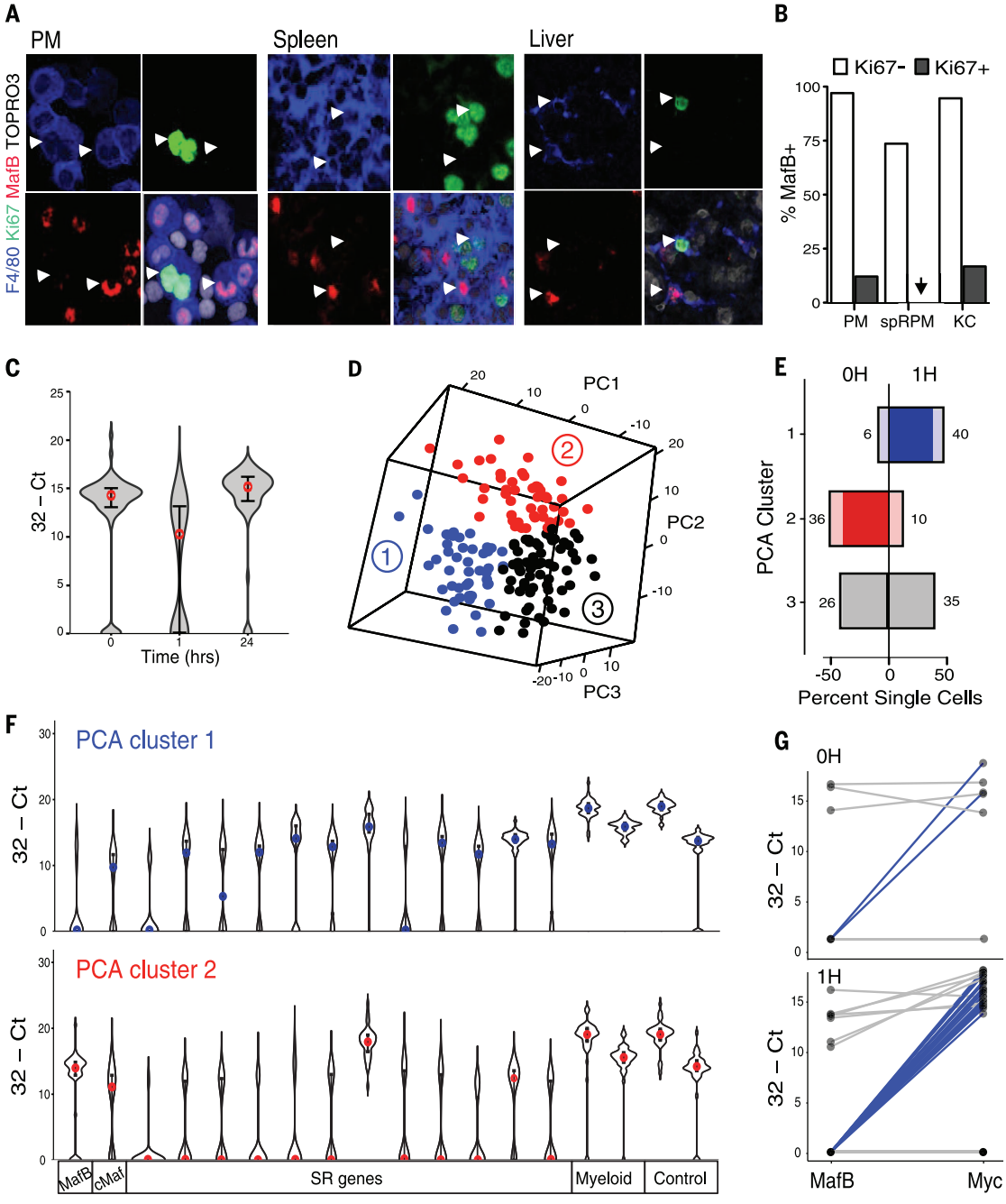

Fig. 7. Single-cell analysis of tissue macrophages in vivo reveals self-renewal gene network activation in MafB-negative macrophages. (**A**) Immunofluorescence images of MafB- and Ki67-positive peritoneal F4/80$^+$ macrophages in cytospun peritoneal macrophages (PMs) and tissue sections from spleen and liver. White arrowheads point to examples of Ki67$^-$/MafB$^+$ and Ki67$^+$/MafB$^-$ macrophages, F4/80$^+$, in each tissue. Data are representative of two independent experiments. Larger-field images are shown in fig. S11. (**B**) Quantification of percent MafB$^+$ cells in the Ki67$^-$ and Ki67$^+$ fraction of F480$^+$/SYTOX blue$^+$ resident macrophages from peritoneum (PMs; n = 969), spleen red pulp macrophages (rpSPM; n = 425), and liver Kupfer cells (KC; n = 302), corresponding to the immunofluorescence images in (A) and fig. S11. Absolute cell counts are shown in table S1. (**C**) Violin plot showing expression of MafB across single PMs isolated from a mouse at the indicated time points after intraperitoneal M-CSF injection, measured by nanofluidic real-time PCR on a Fluidigm array. Red dots mark the median value and error bars the interquartile range. (**D**) Depiction in 3D space of PCA analysis of single-cell gene expression data for a k-means = 3 of pooled data for 0 and 1 hours after M-CSF injection. Distinct PCA clusters are distinguished by colors and numbers. (**E**) Histogram showing the percentage of single cells in each cluster at the 0- and 1-hour time points [clusters as in (D)]. Absolute numbers of cells in each group are indicated, and the net change between 0 and 1 hour is shown in deeper color. (**F**) Violin plots showing expression for Maf, self-renewal (SR), myeloid, and control genes across cells in PCA cluster 1 (blue) and PCA cluster 2 (red) [clusters as in (D)]. Colored dots show the median value and error bars the interquartile range. (**G**) Line diagrams showing individual cell comparison of MafB and Myc expression for PCA cluster 1 at 0 and 1 hours. Single cells with low MafB and high Myc expression are highlighted in blue. Consistent results for (C) to (G) were obtained in a repeat experiment with cells sorted from a pool collected from five mice at each time point.

transcription factors is relieved. In summary, we have shown that self-renewal activity can be activated from an intrinsic cell type–specific enhancer repertoire in differentiated cells. Our findings provide a general molecular rationale for the compatibility of self-renewal and differentiated cell functions and may also be more generally relevant for the activation of self-renewal activity in other differentiated cell types with therapeutic potential.

Materials and methods

Cell culture

Maf-DKO macrophages were grown subconfluently in macrophage growth medium (Dulbecco's modified Eagle's medium with 20% supernatant from L929 mouse fibroblasts, 1% sodium pyruvate, and 1% L-glutamate], as described in (7). WT BMMs were differentiated from total mouse BM for 15 days in macrophage growth medium, selecting for adherent cells every 4 days. For time course analysis of self-renewal gene expression in Maf-DKO and WT BMMs, cells were seeded 18 hours before time 0 in growth medium

without supernatant from L929 mouse fibroblasts; at time 0, 100 ng/ml of recombinant murine stem cell factor (Peprotech) was added to the culture medium; and cells were harvested for RNA isolation and analysis at 0, 1, 2, and 24 hours.

For culture of AMs, alveolar lavages were pooled from 10 1-ml 37°C bronchoalveolar lavage washes [phosphate-buffered saline (PBS) without Mg^{++}/Ca^{++}, 2 mM EDTA, 2% fetal bovine serum (GE Healthcare) per mouse] and stored on ice. Red blood cell (RBC) lysis was then performed at room temperature (RT) for 3 min (RBC Lysis Buffer, Invitrogen). Cells were plated at a density of 1.1 million cells per 10-cm bacterial petri dish in complete medium [RPMI, 10% fetal calf serum (FCS), 1% Pen/Strep, 1% pyruvate, 1% glutamate] supplemented with 1% granulocyte-macrophage CSF (GM-CSF) supernatant from J558L cells transfected with murine GM-CSF cDNA.

MafB expression in Maf-DKO macrophages

The pRetroX-Tet-On Advanced (Clontech, catalog no. 632104) and pRetroX-Tight-Pur (catalog no. 632104) retroviral backbones were used for generating the Flag-tagged MafB-inducible Maf-DKO macrophages. Neo^r was replaced by $Hygro^r$ and $Puro^r$ by green fluorescent protein (GFP) in the pRetroX-Tet-On Advanced and pRetroX-Tight-Pur retroviruses, respectively. Maf-DKO macrophages were first infected with the pRetroX-Tet-On-$hygro^r$ retrovirus and selected for 2 weeks in medium containing 200 μg/ml of Hygromycin B (Life Technologies, catalog no. 10687-010). Selected Maf-DKO macrophages were next infected with the empty pRetroX-Tight-GFP or pRetroX-Tight-GFP containing the Flag-tagged MafB gene cloned downstream of the modified Tet-responsive promoter. GFP-positive Maf-DKO macrophages were then subjected to fluorescence-activated cell sorting (FACS) and cultured in the absence of doxycycline.

Stimulation and isolation of peritoneal macrophages

Either 200 μl of PBS (control) or 20 μg of recombinant M-CSF (Novartis) was injected into the peritoneums of WT C57/B6J 8- to 10-week-old mice at the indicated times before analysis. For cell cycle analysis, mice were also injected intraperitoneally with 2 mg of bromodeoxyuridine (BrdU) (BD Pharmingen) dissolved in PBS, per manufacturer's instructions, 4 hours before analysis. To harvest peritoneal cells, mice were sacrificed and subsequently injected with 10 ml of ice-cold PBS containing 2 mM EDTA (Sigma). Intraperitoneal washouts were collected in 50-ml Falcon tubes. Red cell lysis was performed on total washouts (RBC Lysis Buffer, Invitrogen) before staining for cell surface markers and cell cycle analysis or FACS. The remaining mononuclear cells were then stained using the following antibody cocktail in the presence of FcBlock (BD Biosciences)—CD11b-PE-Cy7 (BD Biosciences); MHC-II-FITC, B220-APC-Cy7, and F4/80-PE (all from eBioscience); and Fixable Aqua Dead-V500 (Life Technologies)—and either sorted for single-cell analysis or further processed for cell cycle analysis.

Cell cycle analysis

Bromodeoxyuridine analysis was performed using a BrdU Flo Kit (BD Pharmingen) according to manufacturer's instructions and with the following modifications: DNaseI digestion was performed for 90 min and intracellular staining for 60 min, and anti-BrdU-AlexaFluor 647 Ab (Invitrogen, clone MoBU-1) was substituted for anti-BrdU provided in the kit. For Ki67 staining, cells were harvested and treated as for BrdU staining but with substitution of an anti-Ki67-V450 antibody (eBiosciences, clone SolA15) for the final incubation step. Cells were analyzed using an LSRII and FlowJo software (Tree Star).

shRNA infections

Lentiviral vector particles were produced at the Centre International de Recherche en Infectiologie (INSERM, UMR 5308 Lyon, France) by tri-transfection of plasmids harboring the packaging construct, the transfer vector (*31*), and the envelope-expressing construct into producer cells using calcium chloride methodology. Virus was concentrated after transfection, and viral supernatants were harvested and used directly for infections or stored at −80°C.

Maf-DKO macrophages were seeded subconfluently in 12-well dishes, 24 hours before infection. The next day, 8 μg/ml of polybrene was incubated for 1.5 hours at 37°C and 5% CO_2 with viral supernatants, and 2 ml per well per infection was used to replace media on Maf-DKO macrophages. Spin infections were carried out at 25°C for 2 hours, with 2500 revolutions per minute (rpm). Viral supernatants were removed immediately after spin infection and replaced with macrophage growth medium. Cells were then further incubated at 37°C and 5% CO_2 for 72 hours before harvesting and divided into fractions for apoptosis, colony assay, and RNA and DNA isolation.

Apoptosis was measured using the Annexin V Apoptosis Detection Kit (eBioscience) according to the manufacturer's instructions. To control for infection, genomic DNA was isolated [using the DNeasy Blood and Tissue Kit (Qiagen)] from infected Maf-DKO cells at 72 hours postinfection. Quantitative polymerase chain reaction (QPCR) was performed to detect the quantity of puromycin cassette contained in the lentiviral vector, relative to a control genomic amplicon [actin transcription start site (TSS)], and to ensure similar infection efficiencies across all populations (fig. S5). Reactions were carried out in a 7500 Real-Time PCR System (Applied Biosystems) including dissociation curves to validate distinct amplicons. RNA was extracted from infected cells and processed for gene expression profiling.

Colony assays

For shRNA-infected cells, 5000 cells were counted from each population of infected cells and mixed with 1 ml of MethoCult medium (M3231, Stem Cell Technologies), with the addition of 100 ng/ml of recombinant M-CSF (Peprotech), plated in duplicate and grown at 37°C, 5% CO_2. For experiments using MafB-inducible Maf-DKO cells, 1000 cells were plated, and 1 μg/ml of doxycycline (Sigma) was added, in addition to M-CSF, where indicated. The number of CFUs was counted on day 12 after plating. Maf-DKO macrophages expressing empty vector (–MafB) or a doxycycline-inducible, Flag-tagged MafB allele (+MafB) were plated at 1000 cells per milliliter of MethoCult medium, as above, with the addition of 1 μg/ml of doxycycline (Sigma). AMs were plated at 10,000 cells per 1 ml of MethoCult M3231 medium (StemCell Technologies) containing 100 ng/ml of recombinant GM-CSF (Peprotech), and colonies were counted after 3 weeks. All experiments were performed with $n = 2$ replicates, and results were reproduced at least three times independently.

In situ immunofluorescent cell staining

PMs were harvested with refrigerated PBS, and 10,000 cells were loaded onto Shandon cytocentrifuge chambers and centrifuged at 1000 rpm for 3 min. Slides were air-dried, fixed with refrigerated 4% paraformaldehyde (PFA) for 10 min at RT, and washed once with PBS. Spleen and liver were harvested after perfusion with PBS and freshly embedded in TissueTeck (OCT Compound) before freezing. Serial frozen sections (8 μm) were fixed with refrigerated 4% PFA for 10 min and washed three times for 5 min with PBS at RT.

Slides were then permeabilized with Triton-X 0.05% (Sigma, catalog no. 9002-93-1) for 10 min and washed three times for 5 min with PBS. Unspecific antigens were blocked for 1 hour with PBS containing 1% FCS, 2% bovine serum albumin (BSA), and 1% goat serum before staining. After blocking, slides were incubated for 1 hour at RT with rabbit anti-mouse MafB (Bethyl, catalog no. IHC-101) diluted at 1:50 and rat anti-mouse Ki67 (eBioscience, catalog no. 14-5698-82) diluted at 1:50 in blocking solution. Slides were subsequently washed three times for 10 min with PBS at RT and incubated with the secondary antibodies donkey anti-rat A488 (Invitrogen, catalog no. A31572) diluted at 1:500 and donkey anti-rabbit A555 (Invitrogen, catalog no. A21208) diluted at 1:500 in PBS. Slides were again washed three times for 10 min with PBS at RT and, finally, incubated for 1 hour with F4/80 A647 (Serotec, catalog no. MCA497A647) diluted at 1:50. A final wash series of three times for 10 min with PBS at RT was performed before mounting with Prolong Gold (Thermo Fischer, catalog no. P36930) with SYTOX Blue diluted at 1:1000 (Thermo Fischer, catalog no. S11348) for nuclear staining. Images were analyzed on a Zeiss LSM510 confocal microscope.

ChIP-seq

Cells cultured in plates were fixed by the direct addition of 1/10 volume of freshly made cross-linking solution (11% formaldehyde, 100 mM NaCl, 1 mM EDTA, 0.5 mM EGTA, 50 mM Hepes at pH 7.8) to cell medium and incubation at RT

for 10 min. Formaldehyde was then quenched for 5 min at RT by the addition of 2.5 M glycine solution to a final concentration of 125 mM. Fixed cells were washed twice with cold PBS, scraped off the plate, counted, and transferred in 50-ml Falcon tubes. Cells were then pelleted by centrifugation at 700*g* for 5 min at 4°C, snap-frozen in liquid nitrogen, and stored at −80°C for storage or shipment on dry ice.

Each batch of 100 million cells was lysed by adding 10 ml of ChIP Lysis Buffer (Santa Cruz Biotechnology, catalog no. sc-45000) or radioimmunoprecipitation assay (RIPA) buffer (1x PBS, 1% NP-40, 0.5% sodium deoxycholate, 0.1% SDS) containing Protease Inhibitor Cocktail (PIC). One complete PIC tablet (Roche, catalog no. 11873580001) for 50 ml of buffer or one mini PIC tablet (Roche, catalog no. 11836153001) for 10 ml of buffer was used. After rotating the cell tube for 10 to 15 min at 4°C, nuclei were pelleted by centrifugation at 700*g* for 5 min at 4°C. Nuclei pellets were resuspended in 5 ml of Santa Cruz Biotechnology ChIP Lysis Buffer High Salt (catalog no. sc-45001) or RIPA buffer containing PIC. Aliquots of 1 ml containing 20 million nuclei were transferred into 1.5-ml low-bind microfuge tubes. The nuclei suspension was either sonicated immediately or snap-frozen in liquid nitrogen and stored at −80°C.

The nuclei-chromatin suspension in each milliliter was sonicated (Sonics Vibra Cell, Model CV188, with Stepped Tip 1/8"-630-0422) on ice in a cold room (4°C). Sonication was performed with nine cycles of 30 s ON at 60% intensity and 30 s OFF for chromosome modifications (H3k4me1 and H3K27ac) or with eight cycles for transcription factors (P300 and PU.1). The sheared chromatin was centrifuged at 14 thousand rpm (krpm) for 10 to 15 min and then transferred (as for the supernatant) into a new 1.5-ml tube and kept on ice for ChIP.

For ChIP, 50-μl Invitrogen Dynabeads (7×10^8 beads/ml) were used for 20 million cells, either anti-rabbit immunoglobulin G (IgG) (catalog no. 112.03D) or anti-mouse IgG (catalog no. 112.01D), depending on the source of the first antibody. The beads were first washed with PBS/BSA/PIC buffer [1x PBS, 5 mg/ml of BSA (Sigma, A3059-10G, Fraction V), Roche PIC (one mini tablet for 10 ml or one complete tablet for 50 ml, added before use)], and then the washed beads were thoroughly resuspended in 1 ml of PBS/BSA/PIC buffer in a 1.5-ml microfuge tube. The tube was placed on a magnetic rack for 1 min, after which the supernatant was removed. This wash was repeated twice by resuspending beads in 1 ml of PBS/BSA/PIC buffer, rotating for 5 min, and removing the supernatant, as described above. The beads were then coated with antibody by resuspending in 250 μl of PBS/BSA/PIC buffer in each tube, adding 5 μg of antibody, and rotating overnight at 4°C. The following antibodies were used: H3K4me1 (Abcam, catalog no. ab8895), H3K4m3 (Abcam, catalog no. ab8580), H3K27ac (Abcam, catalog no. ab4729), P300 (Santa Cruz Biotechnology, catalog no. sc-585), PU.1 (Santa Cruz Biotechnology, catalog no. sc-352), MafB (Bethyl, catalog no. IHC-101), and Flag M2 antibody (Sigma). After overnight incubation with antibody, the beads were pelleted by placing the tube on a magnetic rack for 1 min, followed by removing the supernatant. The beads were then washed three times with PBS/BSA/PIC buffer.

ChIP was carried out by adding the sheared chromatin suspension to the antibody-coated beads and rotating overnight at 4°C, followed by a series of washes. The beads were first washed once with 1 ml of a low-salt wash buffer (20 mM Tris-HCl at pH 8.0, 150 mM NaCl, 2 mM EDTA, 0.1% SDS, 1% Triton X-100), then twice with a high-salt wash buffer (20 mM Tris-HCl at pH 8.0, 500 mM NaCl, 2 mM EDTA, 0.1% SDS, 1% Triton X-100), three times with an LiCl wash buffer (10 mM Tris-HCl at pH 8.0, 250 mM LiCl, 1 mM EDTA, 1% GEPAL CA630, 1% Na-deoxyholate), and twice with TE buffer. ChIP DNA was eluted by adding 200 μl of ChIP Elution Buffer (Santa Cruz Biotechnology, catalog no. sc-45003, or 1% SDS/0.1 M $NaHCO_3$) to each bead tube, vortexing to resuspend beads, and incubating at 65°C for 1 hour with vortexing every 15 min. After beads were centrifuged for 3 min at RT and placed on a magnetic rack for 1 min, ChIP DNA in the supernatant was transferred to a new tube.

Reversal of cross-links was carried out by incubation at 65°C overnight, and DNA was extracted with an equal volume of phenol:chloroform:isoamyl alcohol (24:24:1). After centrifugation at 14 krpm for 3 min, ChIP DNA in the supernatant was transferred to a 2.0-ml low-bind tube. More DNA was extracted by adding 100 μl of water to the phenol:chloroform phase and repeating the extraction. The DNA extract was combined and mixed with five volumes of PBI buffer (5 M GuHCl, 30% isopropanol) Qiagen MinElute PCR Purification Kit, catalog no. 28004). With the use of 3 M NaAc (at pH 5.2), the pH of the mixture was adjusted to <7.5 before the mixture was applied to the column. The mixture turned back to a yellow color, which is important for DNA to bind to the Qiagen column. DNA was purified according to the manufacturer's instructions and eluted in 30 μl of buffer EB. DNA concentration was measured with Qubit (Thermo Fischer). DNA amounts ranging from 30 ng (P300, PU.1, MafB, and Flag-MafB) to 100 ng (H3K4me1 and H3K27ac) were used to make each library.

ChIP-seq libraries were generated using adaptors from Illumina (catalog no. FC102-1001) and other enzymes and reagents from New England BioLabs, following the Illumina ChIP-seq protocol with some minor modifications. ChIP DNA was end-repaired by T4 DNA polymerase (catalog no. M0203S/L), Klenow DNA polymerase (catalog no. M0210S/L), and T4 PNK (catalog no. M0201S/L) and purified with the Qiagen MinElute PCR Purification Kit. A-base was then added to the 3′ end by Klenow Fragment, 3′ to 5′ exo- (New England BioLabs, catalog no. M0212S/L), and deoxyadenosine triphosphate. The Illumina adaptors (1 μl of 1:10 dilution) were subsequently added to both ends by DNA ligase (catalog no. M2200S/L). The adaptor-ligated DNA was size-selected for 200– to 400–base pair (bp) fragments by 2% low-melting agarose gel (Lonza, catalog no. 50080) and was subsequently purified using a Qiagen MinElute Gel Extraction Kit (catalog no. 28604). Library DNA was amplified in a 100-μl reaction by Phusion PCR Master Mix (New England BioLabs, catalog no. F-531S), with primers SolexaPCR_F (5′- AAT GAT ACG GCG ACC ACC GAG ATC TAC ACT CTT TCC CTA CAC GAC GCT CTT CCG ATC T -3′) and SolexaPCR_R (5′- CAA GCA GAA GAC GGC ATA CGA GCT CTT CCG ATC T -3′). Libraries of H3K4me1 and H3K27ac were amplified by predenaturing at 98°C for 30 s; followed by 10 cycles of (i) 98°C for 10 s, (ii) 65°C for 30 s, and (iii) 72°C for 30 s; and then an extra 5 min at 72°C at the end. For the P300 and PU.1 libraries, 12 cycles of PCR were used. After library DNA was purified, library concentration was measured by Qubit, and size distribution was determined by Bioanalyzer (Agilent Technologies). Each ChIP-seq library was sequenced on one lane of Illumina GAIIx or Illumina HiSeq 2000 with 1×36–bases of read length. Biological replicates from two independently derived Maf-DKO macrophage lines (from two different mice) were sequenced, one of which was determined to be tetraploid. Comparison of ChIP-seq and gene expression data revealed no substantive differences between the two lines.

ChIP-seq analysis

Although a DNAnexus pipeline was used for peak detection algorithms (*38*) and alignments of raw data (uploaded fastq files), the aligned data (BAM files) were subsequently downloaded and processed with a custom R pipeline for bioinformatics analyses. A threshold based on the number of sequenced tags (Nseq) has been set up as Nseq/7,000,000. All regions with a number of repeated tags (with identical sequences/coordinates) above this threshold were filtered out to remove possible sequencing and/or alignment artifacts. To accurately represent and further process the ChIP-seq and input control signals, the Watson and Crick strand tags need to be merged after elongation or size extension to the gel-purified fragment size. The optimal elongation size of each ChIP-seq experiment was estimated in silico by employing a stepwise 10-bp chromosomal sequence tag shifting and score multiplication. Tag coordinates were subsequently elongated according to this estimated DNA fragment size, corresponding to the tag shift maximizing the score. Then, a nucleotide score representing the genome-wide overlap of elongated tags was computed across both strands. Wiggle (WIG) files for genome-wide scores were generated after a binning step, and the average enrichment score was calculated every 50 bp.

When input experiments were available, enrichment scores from WIG files were scaled and used as follows: Owing to the size of the genome and the relatively low frequencies of binding events, we assumed that most (>90%) of the obtained scores from the ChIP-seq experiments represent a background (BG) level. We therefore used the genome-wide average

score in each experiment to estimate the BG level. Using these average scores, it is possible to rescale the scores accordingly, acting as normalization and reducing the interexperiment differences due to effects of different sequencing depths and/or fragment sizes.

We employed an input subtraction step for each experiment, using the normalized file for the input control. This step not only allows for correction of overrepresentations of certain genomic regions due to possible (un)favorable events during sonication and/or DNA sequencing but also serves to reduce the signal-to-noise ratio, especially for experiments with low enrichment values.

H3K4me1-enriched regions were extracted from all samples (Maf-DKO, BMMs, PMs, pro-B, ES, liver, and mouse embryonic fibroblasts; annotation files available) (*12*, *13*). All regions close to annotated TSSs (<2 kb) were omitted, and the union of the resulting regions was used as a reference to extract enrichment scores of H3K4me1 derived from all samples. R scripts were developed and used for retrieving bin scores around the center of these annotations (±2 kb). These scores and their original genomic coordinates were utilized to recenter values around the H3K4me1-enriched regions, by means of linear interpolation. In total, 1000 points were interpolated for each selected region, which resulted in a 1000-column matrix. These matrices were loaded, viewed, and color-scaled according to sample read depth using Java TreeView (*39*). Finally, these matrices were assembled by sample.

A large selection of regions enriched for H3K27ac and H3K4me1 was applied to WT and DKO samples. All regions in close proximity to any annotated TSSs (<2 kb) were ignored, and the union of all regions has been defined as putative active enhancers (annotation file available). The binned enrichments of PU.1 samples in these regions were merged and compared among tissues using a nonparametric Spearman correlation method.

Heat maps were created with the same strategy as for fig. S1A (but focused on regions isolated with previously described isolated peaks). For each reference experiment (H3K27ac or P300), the regions were sorted by increasing average enrichment score, and the other heat maps were arranged with respect to this initial sorting for corresponding experiments.

For the heat map in Fig. 4B, SRA files for ES cell ChIP-seq data (*13*) were converted into FASTQ format before being uploaded and processed on the DNAnexus platform. Two replicate H3K27ac ES cell ChIP-seq BAM files were merged, and BAM files were then processed by DNAnexus, as described above. All reads from BAM files with a MAPQ (MAPping Quality) value <10 were filtered out so that only confidently mapped reads were retained. The numbers of reads in each relevant region were counted according to their start position. Each read with a start position outside the region was not taken into account, regardless of the strand considered.

The read-counts matrix was normalized by considering each mark independently of the others. For each antibody, the number of reads for each region was normalized relative to the total number of confidently mapped reads of the least-sequenced sample. Because these regions are not homogeneous in length, counts were normalized to the size of the region in kilo–base pairs. Next, considering each antibody independently, counts exceeding the 95th percentile were set to this value to avoid bias due to outliers. Values were then set to the range 0 to 1 and sorted according to the Maf-DKO region's H3K27ac level. Finally a 2-means clustering (k = 2) was performed on H3K27ac marks for the three cell types (Maf-DKO macrophages, WT BMMs, and ES cells). The analysis depicted in Fig. 6E used the same approach for PU.1 and p300 marks in Maf-DKO macrophages, WT BMMs, and AMs. All analyses were performed using Samtools, R (version 2.14), and gene-e (version 3.0.202).

Motif search at enhancer loci

Motifs analysis was performed using HOMER2 (http://homer.salk.edu/homer/) on 10,232 DKO-only peaks (the union of H3K27ac and P300 selection based on enrichment in Maf-DKO macrophages versus WT BMMs) and 88 self-renewal gene–associated peaks from within the DKO-only selection. Among other things, HOMER2 screens for enrichment of known motifs. The HOMER perl script findMotifsGenome.pl was used with the mm9 mouse genome as a background (random genomic sequences sampled according to GC content of input sequences).

GSEA analysis

Maf-DKO versus WT log2 ratios were computed for each probe set from normalized data by RMA method (robust multiarray average). H3K27ac DKO-only regions and P300 DKO-only peaks were associated with nearby genes via GREAT (http://bejerano.stanford.edu/great/public/html/index.php) (*20*).

Next, the union of DKO-only enhancer–associated genes was considered. For the purposes of GSEA (www.broad.mit.edu/gsea), 7499 Maf-DKO–versus–WT ratios of these non-unique DKO-only enhancer–associated genes (a gene can have multiple associated probe sets) were selected. Two stem cell modules were used as gene sets: (i) an adult tissue stem module regrouping genes coordinately up-regulated in a compendium of mouse adult tissue stem cells and (ii) a second module composed of genes coordinately up-regulated in mouse ES cells, as defined in (*21*). These two sets were extracted from the public Molecular Signatures Database (MSigDB) (www.broadinstitute.org/gsea/msigdb/index.jsp).

Single-cell– and bulk cell–population gene expression profiling and analysis

Single cells were sorted, using the autoclone module on an AriaIII sorter (Becton Dickinson), directly into 96-well plates in the CellsDirect Reaction Mix (Invitrogen). Individual cell lysis, cDNA synthesis, and amplification were carried out via single-cell microfluidic real-time PCR using Dynamic Array integrated fluidic circuits (IFCs) (Biomark Fluidigm), according to the Fluidigm Advanced Development Protocol. Preamplified products (20 cycles) were diluted by a factor of 5 before analysis with Universal PCR Master Mix and inventoried TaqMan gene expression assays (Applied Biosystems) in 96.96 Dynamic Arrays on a BioMark System (Fluidigm). For single-cell analysis, cycle threshold (Ct) values were calculated from the system's software (BioMark Real-time PCR Analysis, Fluidigm) and filtered according to a set of quality control rules (outlined below).

For single-cell gene expression level analysis, the raw data were preprocessed as follows: For each gene, including controls, those with a difference of duplicate Ct values ≥2.0 were considered inconsistent and removed. If the control gene (*GAPDH*) was not expressed or filtered out, the whole sample was removed. If Ct_{Call} = FAILED but the sample showed expression of at least one other gene, it was considered as "not expressed," and the Ct value was set to 31.9. The relative expression values were calculated according to the following formula: relative expression = 32 – mean (technical replicates).

R scripts with the ggplot2 package were used to construct violin plots and line plots on relative expression values. Results shown in the figures are representative of two independent experiments.

The RGL package was used for PCA to cluster relative expression values on a three-dimensional (3D) principal component space. PCA coordinates were clustered by the k-means method (*40*) using R script.

For bulk cell populations, total RNA was isolated from cells using the Quiagen RNAeasy kit and treated with RNAse-free DNAseI (Qiagen) before elution from columns. For gene expression profiling, RNA from Maf-DKO macrophages was extracted using the RNeasy Mini Kit (Qiagen) and QIAshredder columns (Qiagen) according to the manufacturer's instructions. On-column DNA digestion was performed. Total RNA (50 ng) was used for reverse transcription to cDNA using SuperScriptTM II RT (Invitrogen), Oligo(dT) primers (Invitrogen), and RNaseOUT (Invitrogen). Specific gene target amplification was performed according to Fluidigm protocols. Selected TaqMan Gene Expression assays (20x) were pooled and diluted with water by a factor of 100, so that each assay is at a final concentration of 0.2x in the pooled assay mix. For preamplification of each cDNA sample, 1.25 μl of the respective cDNA, 1.25 μl of pooled assay mix, and 2.5 μl of TaqMan PreAmp Master Mix (Applied Biosystems, catalog no. 4391128) were combined to a final volume of 5 μl in 1 well of a 96-well QPCR plate. cDNA samples were amplified using the following program: (i) 95°C for 10 min, (ii) 95°C for 15 s, and (iii) 60°C for 4 min; then repeat steps (ii) and (iii) 14 times. Amplified cDNA samples were diluted at 1:5 using 20 μl of water. For Fluidigm 96.96 Dynamic Array IFC analysis, 5 μl of each cDNA sample and 5 μl of each TaqMan probe (20x) were loaded on the chip.

Microfluidic real-time PCR using Dynamic Array IFCs (Biomark Fluidigm) was performed

with Universal PCR Master Mix and inventoried TaqMan gene expression assays (Applied Biosystems) in 96.96 Dynamic Arrays on a BioMark System (Fluidigm). Ct values were calculated from the system's software (BioMark Real-time PCR Analysis, Fluidigm) and filtered according to a set of quality control rules (outlined below).

Gene filter: (i) For each gene, including controls, data with Ct_{Call} = FAILED and $Ct_{Quality}$ < threshold were removed. (ii) For each gene, including controls, only Ct values that met the following criterion were considered: at least 2.0 below the lowest Ct value of no-RT or no-RNA controls. The purpose of this was to filter out inefficient probes and genes with very low expression. (iii) For each gene, including controls, values with a difference ≥2.0 between Ct_{max} and Ct_{min} of replicates were considered to be inconsistent and were removed. (iv) If a gene was removed [according to filters (i) to (iii)] from uninfected or control shRNA samples, it was removed from all samples. Sample filter: (i) If the control gene (*GAPDH*) was not expressed or was removed according to gene filters (i) to (iii), the whole sample was removed. (ii) If a control gene (*GAPDH*) had a Ct value with a ≥2.0 difference from the average Ct value of control genes in all samples, the whole sample was removed to eliminate nonspecific shRNA and normalization artifacts. For the heat map, each Ct value was normalized against *GAPDH* using the following formula: relative $\text{expression}_{Sample} = 2^{[\text{mean}(Ct_{GAPDH}) - Ct_{Sample}]} \times 100$. For each gene, heat maps in Fig. 2C present normalized values as percent change over average expression in noninfected and control lacZ shRNA–infected cell samples.

Furthermore, z scores were calculated for each gene of shRNA-infected cell samples based on uninfected and lacZ control shRNA–infected samples, as described in (*31*). Briefly, a statistic z was defined for each observation o_{ij} of transcript i in each shRNA experiment j

$$z_{ij} = \frac{o_{ij} - m_i}{s_i}$$

where m_i and s_i are, respectively, the mean and variance of the expression of transcript i in the control experiments (uninfected and lacZ shRNAs).

Two false discovery rate (FDR)–based approaches were used to obtain confidence estimates of the observed z scores. First, a per-gene confidence score was defined by using the variation of that gene's expression in the control shRNA experiments. Permuted scores z_k^{ij} (where k is the number of permutations) as a null distribution and the FDR for a given z score z_{ij} for gene i in experiment j are given as

$$FDR_i(z) = \frac{E_k(\#\{z_k^{ij} | z_k^{ij} \rangle z; j \in P\})}{\#\{z^{ij} > z; j = 1, \ldots, n\}}$$

where n is the number of shRNA experiments, E is the expectation, the confidence for z is $conf(z) = 1 - FDR(z)$, and $P = \{c | z^{ic} \rangle z; c = 1, \ldots, n\}$.

In the second approach, we defined a per-shRNA confidence score for each measurement of a self-renewal gene by calculating an FDR based on the variation of expression in *GAPDH* and myeloid genes. Formally, we let $z_{ij},\ldots,z_{nj}$ be the scores for the jth experiment (shRNA) and assumed the first l transcripts were control transcripts whose expression did not change in response to any component. We defined $\tilde{z}_{ij} = \frac{z_{ij} - \tilde{m}_j}{\tilde{s}_j}$ where now $\tilde{m}_j$ and $\tilde{s}_j$ are, respectively, the mean and variance of the z scores of the control transcripts $1,\ldots,l$ in the jth shRNA experiment. We performed l permutations, as described above, by swapping each observed z score with a control transcript score and computing z, then computing an FDR as above. For the construction of the network model, we considered only values with an FDR <0.05 and where at least half of the replicates fulfilled these criteria. Circle sizes reflect the number of times the expression of a gene is affected by the perturbation of another gene, scoring each gene and shRNA replicate separately.

For time-course analysis of self-renewal gene expression in Maf-DKO macrophages and WT BMMs, values were obtained by subtracting the considered gene mean across all samples from an individual raw score and then dividing the difference by the considered gene SD across all samples. Statistical analysis was performed using R (version 2.14), heat maps were created using the software gene-e (Broad Institute), and network diagrams were generated with Cytoscape (version 3.0.2).

Construction of self-renewal gene network

To investigate the potential for cross-regulation between self-renewal genes, data from a quadruplicate nanofluidic real-time PCR on Fluidigm array, presented in Fig. 2C, were reanalyzed, and z score computations were used to decide whether a given shRNA regulated its specific target mRNA and whether this regulation affected the expression of other genes (control or self-renewal genes). Computations were performed according to per-gene and per-shRNA computation methods, as described above and with the following additional considerations: (i) With the exception of Myc and Chd1, for which only one shRNA was found to effectively knock down the expression of said target, all self-renewal genes were effectively targeted by two shRNAs. Therefore, to balance the number of replicates per sample so as not to undercount the number of regulations relative to other shRNAs, all of the regulations where shMyc and shChd1 were involved were counted twice for subsequent computations. (ii) The regulation of a gene upon expression of a given shRNA was not taken into account unless more than two replicates for gene expression were significantly regulated, regardless of the computation method considered. This concerned only 13 of 86 regulations that were subsequently filtered out for the per-gene computation and none for the per-shRNA computation. (iii) All autoregulations (shGene-x regulating Gene-x) were considered trivial and were thus removed. (iv) Baseline expression of all genes was determined according to average expression levels in control samples.

Together, these data were used to construct a gene regulation network (depicted in Fig. 3B). The size of the bubble for each gene in the network was drawn relative to the number of times the gene was regulated by an shRNA for which it was not the direct target. A line was drawn to connect genes when the shRNA regulated the expression of a nontarget RNA at least two of the four times tested for at least one of two shRNAs in both computations. Given that there are two shRNAs per gene, four gene expression replicates, and two computation methods, 16 regulations could be evaluated for a given shRNA. When all 16 regulations were significant and the same, the lines in Fig. 3B were drawn in black; otherwise, they were drawn in gray. The red end of the arrows indicates a repression of the gene by the shRNA, whereas the blue end indicates activation. Genes targeted only by shRNA with statistical significance in only one computation (single nodes) were not represented.

REFERENCES AND NOTES

1. S. J. Jenkins *et al.*, Local macrophage proliferation, rather than recruitment from the blood, is a signature of T_H2 inflammation. *Science* **332**, 1284–1288 (2011). pmid: 21566158
2. C. Schulz *et al.*, A lineage of myeloid cells independent of Myb and hematopoietic stem cells. *Science* **336**, 86–90 (2012). doi: 10.1126/science.1219179; pmid: 22442384
3. S. Yona *et al.*, Fate mapping reveals origins and dynamics of monocytes and tissue macrophages under homeostasis. *Immunity* **38**, 79–91 (2013). pmid: 23273845
4. D. Hashimoto *et al.*, Tissue-resident macrophages self-maintain locally throughout adult life with minimal contribution from circulating monocytes. *Immunity* **38**, 792–804 (2013). doi: 10.1016/j.immuni.2013.04.004; pmid: 23601688
5. M. H. Sieweke, J. E. Allen, Beyond stem cells: Self-renewal of differentiated macrophages. *Science* **342**, 1242974 (2013). doi: 10.1126/science.1242974; pmid: 24264994
6. E. L. Gautier *et al.*, Gene-expression profiles and transcriptional regulatory pathways that underlie the identity and diversity of mouse tissue macrophages. *Nat. Immunol.* **13**, 1118–1128 (2012).pmid: 23023392
7. A. Aziz, E. Soucie, S. Sarrazin, M. H. Sieweke, MafB/c-Maf deficiency enables self-renewal of differentiated functional macrophages. *Science* **326**, 867–871 (2009). doi: 10.1126/science.1176056; pmid: 19892988
8. G. Fejer *et al.*, Nontransformed, GM-CSF-dependent macrophage lines are a unique model to study tissue macrophage functions. *Proc. Natl. Acad. Sci. U.S.A.* **110**, E2191–E2198 (2013). doi: 10.1073/pnas.1302877110; pmid: 23708119
9. N. D. Heintzman *et al.*, Histone modifications at human enhancers reflect global cell-type-specific gene expression. *Nature* **459**, 108–112 (2009). doi: 10.1038/nature07829; pmid: 19295514
10. G. Natoli, Maintaining cell identity through global control of genomic organization. *Immunity* **33**, 12–24 (2010). doi: 10.1016/j.immuni.2010.07.006; pmid: 20643336
11. S. Ghisletti *et al.*, Identification and characterization of enhancers controlling the inflammatory gene expression program in macrophages. *Immunity* **32**, 317–328 (2010). doi: 10.1016/j.immuni.2010.02.008; pmid: 20206554
12. S. Heinz *et al.*, Simple combinations of lineage-determining transcription factors prime cis-regulatory elements required for macrophage and B cell identities. *Mol. Cell* **38**, 576–589 (2010). doi: 10.1016/j.molcel.2010.05.004; pmid: 20513432
13. M. P. Creyghton *et al.*, Histone H3K27ac separates active from poised enhancers and predicts developmental state. *Proc. Natl. Acad. Sci. U.S.A.* **107**, 21931–21936 (2010). doi: 10.1073/pnas.1016071107; pmid: 21106759
14. G. Natoli, J. C. Andrau, Noncoding transcription at enhancers: General principles and functional models. *Annu. Rev. Genet.* **46**, 1–19 (2012). doi: 10.1146/annurev-genet-110711-155459; pmid: 22905871

15. D. Gosselin *et al*., Environment drives selection and function of enhancers controlling tissue-specific macrophage identities. *Cell* **159**, 1327–1340 (2014). doi: 10.1016/j.cell.2014.11.023; pmid: 25480297
16. Y. Lavin *et al*., Tissue-resident macrophage enhancer landscapes are shaped by the local microenvironment. *Cell* **159**, 1312–1326 (2014). pmid: 25480296
17. R. Ostuni *et al*., Latent enhancers activated by stimulation in differentiated cells. *Cell* **152**, 157–171 (2013). doi: 10.1016/j.cell.2012.12.018; pmid: 23332752
18. A. Visel *et al*., ChIP-seq accurately predicts tissue-specific activity of enhancers. *Nature* **457**, 854–858 (2009). doi: 10.1038/nature07730; pmid: 19212405
19. A. Rada-Iglesias *et al*., A unique chromatin signature uncovers early developmental enhancers in humans. *Nature* **470**, 279–283 (2011). doi: 10.1038/nature09692; pmid: 21160473
20. C. Y. McLean *et al*., GREAT improves functional interpretation of cis-regulatory regions. *Nat. Biotechnol.* **28**, 495–501 (2010). doi: 10.1038/nbt.1630; pmid: 20436461
21. D. J. Wong *et al*., Module map of stem cell genes guides creation of epithelial cancer stem cells. *Cell Stem Cell* **2**, 333–344 (2008). doi: 10.1016/j.stem.2008.02.009; pmid: 18397753
22. N. Ivanova *et al*., Dissecting self-renewal in stem cells with RNA interference. *Nature* **442**, 533–538 (2006). doi: 10.1038/nature04915; pmid: 16767105
23. J. Z. Zhang *et al*., Screening for genes essential for mouse embryonic stem cell self-renewal using a subtractive RNA interference library. *Stem Cells* **24**, 2661–2668 (2006). doi: 10.1634/stemcells.2006-0017; pmid: 16960129
24. M. Pritsker, N. R. Ford, H. T. Jenq, I. R. Lemischka, Genomewide gain-of-function genetic screen identifies functionally active genes in mouse embryonic stem cells. *Proc. Natl. Acad. Sci. U.S.A.* **103**, 6946–6951 (2006). doi: 10.1073/pnas.0509861103; pmid: 16621925
25. J. Hall *et al*., Oct4 and LIF/Stat3 additively induce Krüppel factors to sustain embryonic stem cell self-renewal. *Cell Stem Cell* **5**, 597–609 (2009). doi: 10.1016/j.stem.2009.11.003; pmid: 19951688
26. J. Jiang *et al*., A core Klf circuitry regulates self-renewal of embryonic stem cells. *Nat. Cell Biol.* **10**, 353–360 (2008). doi: 10.1038/ncb1698; pmid: 18264089
27. A. Gaspar-Maia *et al*., Chd1 regulates open chromatin and pluripotency of embryonic stem cells. *Nature* **460**, 863–868 (2009).pmid: 19587682
28. G. Hu *et al*., A genome-wide RNAi screen identifies a new transcriptional module required for self-renewal. *Genes Dev.* **23**, 837–848 (2009). doi: 10.1101/gad.1769609; pmid: 19339689
29. L. Ding *et al*., A genome-scale RNAi screen for Oct4 modulators defines a role of the Paf1 complex for embryonic stem cell identity. *Cell Stem Cell* **4**, 403–415 (2009). doi: 10.1016/j.stem.2009.03.009; pmid: 19345177
30. B. D. Macarthur, A. Ma'ayan, I. R. Lemischka, Systems biology of stem cell fate and cellular reprogramming. *Nat. Rev. Mol. Cell Biol.* **10**, 672–681 (2009). pmid: 19738627
31. I. Amit *et al*., Unbiased reconstruction of a mammalian transcriptional network mediating pathogen responses. *Science* **326**, 257–263 (2009). doi: 10.1126/science.1179050; pmid: 19729616
32. Y. Bakri *et al*., Balance of MafB and PU.1 specifies alternative macrophage or dendritic cell fate. *Blood* **105**, 2707–2716 (2005). doi: 10.1182/blood-2004-04-1448; pmid: 15598817
33. R. Gentek, K. Molawi, M. H. Sieweke, Tissue macrophage identity and self-renewal. *Immunol. Rev.* **262**, 56–73 (2014). doi: 10.1111/imr.12224; pmid: 25319327
34. L. C. Davies *et al*., Distinct bone marrow-derived and tissue-resident macrophage lineages proliferate at key stages during inflammation. *Nat. Commun.* **4**, 1886 (2013). doi: 10.1038/ncomms2877; pmid: 23695680
35. S. J. Jenkins *et al*., IL-4 directly signals tissue-resident macrophages to proliferate beyond homeostatic levels controlled by CSF-1. *J. Exp. Med.* **210**, 2477–2491 (2013). doi: 10.1084/jem.20121999; pmid: 24101381
36. J. A. Hamilton, G. A. Whitty, I. Kola, P. J. Hertzog, Endogenous IFN-alpha beta suppresses colony-stimulating factor (CSF)-1-stimulated macrophage DNA synthesis and mediates inhibitory effects of lipopolysaccharide and TNF-alpha. *J. Immunol.* **156**, 2553–2557 (1996). pmid: 8786318
37. H. Motohashi, K. Igarashi, MafB as a type I interferon rheostat. *Nat. Immunol.* **11**, 695–696 (2010). doi: 10.1038/ni0810-695; pmid: 20644578
38. A. Valouev *et al*., Genome-wide analysis of transcription factor binding sites based on ChIP-Seq data. *Nat. Methods* **5**, 829–834 (2008). doi: 10.1038/nmeth.1246; pmid: 19160518
39. A. J. Saldanha, Java Treeview—Extensible visualization of microarray data. *Bioinformatics* **20**, 3246–3248 (2004). doi: 10.1093/bioinformatics/bth349; pmid: 15180930
40. J. A. Hartigan, M. A. Wong, A *K*-means clustering algorithm. *J. R. Stat. Soc. C Appl. Stat.* **28**, 100–108 (1979).

ACKNOWLEDGMENTS

We thank N. Spies for advice on statistical analysis, L. Chasson for immunofluorescence processing, and S. Vargas-Aguilar for reagents. The data presented in this manuscript are tabulated in the main paper and in the supplementary materials. Sequencing data can be accessed in Gene Expression Omnibus under accession number GSE75722. E.L.S. received fellowships from the European Union Marie Curie program and La Fondation de France. E.L.S. and P.D. were supported by La Ligue Nationale Contre le Cancer (Equipe Labelisée), K.M. by a Human Frontier Science Program long-term fellowship and Stiftung Charité, L.G. by the Fondation ARC pour la Recherche sur le Cancer, J.-C.A. by the Fondation pour la Recherche Médicale (grant AJE20130728183), A.S. by the NIH National Institute on Aging (grant P01AG036695), and M.H.S. by the Agence Nationale de la Recherche (grant ANR-11-BSV3-026-01) and Institut National du Cancer (grant 13-10/405/AB-LC-HS). M.H.S. is an Einstein-BIH fellow and Fondation pour la Recherche Médicale (grant DEQ20110421320) and INSERM-Helmholtz group leader.

SUPPLEMENTARY MATERIALS

www.sciencemag.org/content/351/6274/aad5510/suppl/DC1
Figs. S1 to S13
Tables S1 to S4
References

29 September 2015; accepted 22 December 2015
Published online 21 January 2016;
10.1126/science.aad5510

Lineage-specific enhancers activate self-renewal genes in macrophages and embryonic stem cells

Erinn L. Soucie *et al.*

Science **351**, (2016);
DOI: 10.1126/science.aad5510

Science (print ISSN 0036-8075; online ISSN 1095-9203) is published weekly, except the last week in December, by the American Association for the Advancement of Science, 1200 New York Avenue NW, Washington, DC 20005.